Chapter 1

TYRE CHARACTERISTICS AND VEHICLE HANDLING AND STABILITY

1.1. Introduction

This chapter is meant to serve as an introduction to vehicle dynamics with emphasis on the influence of tyre properties. Steady-state cornering behaviour of simple automobile models and the transient motion after small and large steering inputs and other disturbances will be discussed. The effects of various shape factors of tyre characteristics (cf. Fig.1.1) on vehicle handling properties will be analysed. The slope of the side force F_y vs slip angle α near the origin (the cornering or side slip stiffness) is the determining parameter for the basic linear handling and stability behaviour of automobiles. The possible offset of the tyre characteristics with respect to their origins may be responsible for the occurrence of the so-called tyre-pull phenomenon. The further non-linear shape of the side (or cornering) force characteristic governs the handling and stability properties of the vehicle at higher lateral accelerations. The load dependency of the curves, notably the non-linear relationship of cornering stiffness with tyre normal load has a considerable effect on the handling characteristic of the car. For the (quasi)

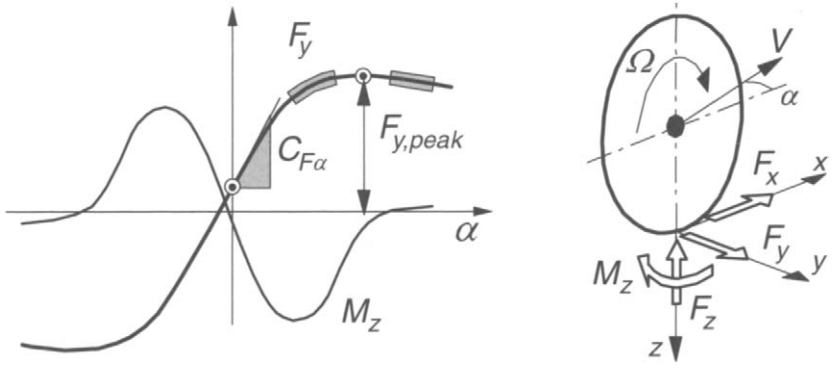

Fig. 1.1. Characteristic shape factors (indicated by points and shaded areas) of tyre or axle characteristics that may influence vehicle handling and stability properties. Slip angle and force and moment positive directions, cf. App.1.

steady-state handling analysis simple single track (two-wheel) vehicle models will be used. Front and rear axle effective side force characteristics are introduced to represent effects that result from suspension and steering system design factors such as steering compliance, roll steer and lateral load transfer. Also the effect of possibly applied (moderate) braking and driving forces may be incorporated in the effective characteristics. Large braking forces may result in wheel lock and possibly large deviations from the undisturbed path. The motion resulting from wheel lock will be dealt with in an application of the theory of a simple physical tyre model in Chapter 3 (the brush model). The application of the handling and stability theory to the dynamics of heavy trucks will also be briefly dealt with in the present chapter. Special attention will be given to the phenomenon of oscillatory instability that may show up with the car trailer combination.

When the wavelength of an oscillatory motion of the vehicle that may arise from road unevenness, brake torque fluctuations, wheel unbalance or instability (shimmy), is smaller than say 5m, a non-steady-state or transient description of tyre response is needed to properly analyse the phenomenon. In Chapters 5-8 these matters will be addressed. Applications demonstrate the use of transient and oscillatory tyre models and provide insight into the vehicle dynamics involved. Chapter 11 is specially devoted to the analysis of motorcycle cornering behaviour and stability.

1.2. Tyre and Axle Characteristics

Tyre characteristics are of crucial importance for the dynamic behaviour of the road vehicle. In this section an introduction is given to the basic aspects of the force and moment generating properties of the pneumatic tyre. Both the pure and combined slip characteristics of the tyre are discussed and typical features presented. Finally, the so-called effective axle characteristics are derived from the individual tyre characteristics and the relevant properties of the suspension and steering system.

1.2.1. Introduction to Tyre Characteristics

The upright wheel rolling freely, that is without applying a driving torque, over a flat level road surface along a straight line at zero side slip, may be defined as the starting situation with all components of slip equal to zero. A relatively small pulling force is needed to overcome the tyre rolling resistance and a side force

and (self) aligning torque may occur as a result of the not completely symmetric structure of the tyre. When the wheel motion deviates from this by definition zero slip condition, wheel slip occurs that is accompanied by a build-up of additional tyre deformation and possibly partial sliding in the contact patch. As a result, (additional) horizontal forces and the aligning torque are generated. The mechanism responsible for this is treated in detail in the subsequent chapters. For now, we will suffice with some important experimental observations and define the various slip quantities that serve as inputs into the tyre system and the moment and forces that are the output quantities (positive directions according to Fig.1.1). Several alternative definitions are in use as well. In Appendix 1 various sign conventions of slip, camber and output forces and moments together with relevant characteristics have been presented.

For the freely rolling wheel the forward speed V_x (longitudinal component of the total velocity vector V of the wheel centre) and the angular speed of revolution Ω_o can be taken from measurements. By dividing these two quantities the so-called effective rolling radius r_e is obtained:

$$r_e = \frac{V_x}{\Omega_o} \tag{1.1}$$

Although the effective radius may be defined also for a braked or driven wheel, we restrict the definition to the case of free rolling. When a torque is applied about the wheel spin axis a longitudinal slip arises that is defined as follows:

$$\kappa = -\frac{V_x - r_e\Omega}{V_x} = -\frac{\Omega_o - \Omega}{\Omega_o} \tag{1.2}$$

The sign is taken such that for a positive κ a positive longitudinal force F_x arises, that is: a driving force. In that case, the wheel angular velocity Ω is increased with respect to Ω_o and consequently $\Omega > \Omega_o = V_x/r_e$. During braking, the fore and aft slip becomes negative. At wheel lock, obviously, $\kappa = -1$. At driving on slippery roads, κ may attain very large values. To limit the slip to a maximum equal to one, in some texts the longitudinal slip is defined differently in the driving range of slip: in the denominator of (1.2) Ω_o is replaced by Ω. This will not be done in the present text.

Lateral wheel slip is defined as the ratio of the lateral and the forward velocity of the wheel. This corresponds to minus the tangent of the slip angle α (Fig.1.1). Again, the sign of α has been chosen such that the side force becomes positive at positive slip angle.

$$\tan\alpha = -\frac{V_y}{V_x} \tag{1.3}$$

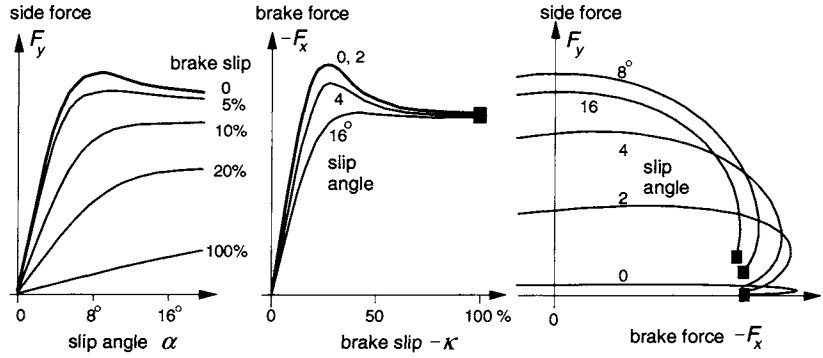

Fig. 1.2. Combined side force and brake force characteristics.

The third and last slip quantity is the so-called spin which is due to rotation of the wheel about an axis normal to the road. Both the yaw rate resulting in path curvature when α remains zero, and the wheel camber or inclination angle γ of the wheel plane about the x axis contribute to the spin. The camber angle is defined positive when looking from behind the wheel is tilted to the right. In Chapter 2 more precise definitions of the three components of wheel slip will be given. The forces F_x and F_y and the aligning torque M_z are results of the input slip. They are functions of the slip components and the wheel load. For steady-state rectilinear motions we have in general:

$$F_x = F_x(\kappa, \alpha, \gamma, F_z)\ ,\ F_y = F_y(\kappa, \alpha, \gamma, F_z)\ ,\ M_z = M_z(\kappa, \alpha, \gamma, F_z) \qquad (1.4)$$

The vertical load F_z may be considered as a given quantity that results from the normal deflection of the tyre. The functions can be obtained from measurements for a given speed of travel and road and environmental conditions.

Figure 1.1 shows the adopted system of axes (x, y, z) with associated positive directions of velocities and forces and moments. The exception is the vertical force F_z acting from road to tyre. For practical reasons, this force is defined to be positive in the upward direction and thus equal to the normal load of the tyre. Also Ω (not provided with a y subscript) is defined positive with respect to the negative y axis. Note, that the axes system is in accordance with SAE standards (SAE J670e 1976). The sign of the slip angle, however, is chosen opposite with respect to the SAE definition, cf. Appendix 1.

In Fig. 1.2 typical pure lateral ($\kappa = 0$) and longitudinal ($\alpha = 0$) slip characteristics have been depicted together with a number of combined slip curves. The camber angle γ was kept equal to zero. We define pure slip to be the situation when either longitudinal or lateral slip occurs in isolation. The figure indicates that a drop in force arises when the other slip component is added. The resulting situation is designated as combined slip. The decrease in force can be simply

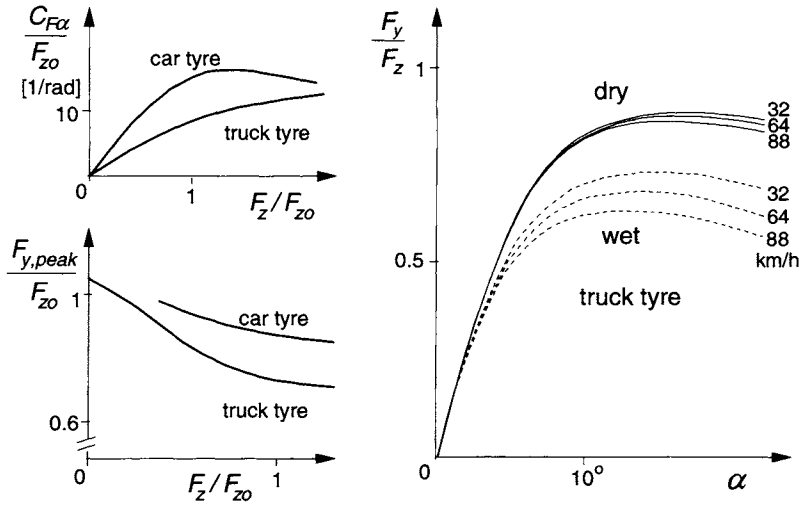

Fig. 1.3. Typical characteristics for the normalised cornering stiffness, peak side force and side force vs normalised vertical load and slip angle respectively. F_{zo} is the rated load.

explained by realising that the total horizontal frictional force F cannot exceed the maximum value (radius of 'friction circle') which is dictated by the current friction coefficient and normal load. Later, in Chapter 3 this becomes clear when considering the behaviour of a simple physical tyre model. The diagrams include the situation when the brake slip ratio has finally attained the value 100% ($\kappa = -1$) which corresponds to wheel lock.

The slopes of the pure slip curves at vanishing slip are defined as the longitudinal and lateral slip stiffnesses respectively. The longitudinal slip stiffness is designated as $C_{F\kappa}$. The lateral slip or cornering stiffness of the tyre, denoted with $C_{F\alpha}$, is one of the most important property parameters of the tyre and is crucial for the vehicle's handling and stability performance. The slope of minus the aligning torque versus slip angle curve (Fig.1.1) at zero slip angle is termed as the aligning stiffness and is denoted with $C_{M\alpha}$. The ratio of minus the aligning torque and the side force is the pneumatic trail t (if we neglect the so-called residual torque to be dealt with in Chapter 4). This length is the distance behind the contact centre (projection of wheel centre onto the ground in wheel plane direction) to the point where the resulting lateral force acts. The linearised force and moment characteristics (valid at small levels of slip) can be represented by the following expressions in which the effect of camber has been included:

$$\begin{aligned} F_x &= C_{F\kappa}\kappa \\ F_y &= C_{F\alpha}\alpha + C_{F\gamma}\gamma \\ M_z &= -C_{M\alpha}\alpha + C_{M\gamma}\gamma \end{aligned} \tag{1.5}$$

These equations have been arranged in such a way that all the coefficients (the force and moment slip and camber stiffnesses) become positive quantities.

It is of interest to note that the order of magnitude of the tyre cornering stiffness ranges from about 6 to about 30 times the vertical wheel load when the cornering stiffness is expressed as force per radian. The lower value holds for the older bias-ply tyre construction and the larger value for modern racing tyres. The longitudinal slip stiffness has been typically found to be about 50% larger than the cornering stiffness. The pneumatic trail is approximately equal to a quarter of the contact patch length. The dry friction coefficient usually equals ca.0.9, on very sharp surfaces and on clean glass ca. 1.6; racing tyres may reach 1.5 to 2.

For the side force which is the more important quantity in connection with automobile handling properties, a number of interesting diagrams have been presented in Fig.1.3. These characteristics are typical for truck and car tyres and are based on experiments conducted at the University of Michigan Transportation Research Institute (UMTRI, formerly HSRI), cf. Ref. (Segel et al. 1981). The car tyre cornering stiffness data stems from newer findings. It is seen that the cornering stiffness changes in a less than proportional fashion with the normal wheel load. The maximum normalised side force $F_{y,peak}/F_z$ appears to decrease with increasing wheel load. Marked differences in level and slope occur for the car and truck tyre curves also when normalised with respect to the rated or nominal load. The cornering force vs slip angle characteristic shown at different speeds and road conditions indicate that the slope at zero slip angle is not or hardly affected by the level of speed and by the condition wet or dry. The peak force level shows only little variation if the road is dry. On a wet road a more pronounced peak occurs and the peak level drops significantly with increasing speed.

Curves which exhibit a shape like the side force characteristics of Fig.1.3 can be represented by a mathematical formula that has become known by the name *'Magic Formula'*. A full treatment of the empirical tyre model associated with this formula is given in Chapter 4. For now we can suffice with showing the basic expressions for the side force and the cornering stiffness:

$$F_y = D \sin[C \arctan\{B\alpha - E(B\alpha - \arctan(B\alpha))\}]$$

with stiffness factor

$$B = C_{F\alpha}/(CD)$$

peak factor (1.6)

$$D = \mu F_z \quad (= F_{y,peak})$$

and cornering stiffness

$$C_{F\alpha} (= BCD) = c_1 \sin\{2 \arctan(F_z/c_2)\}$$

The shape factors C and E as well as the parameters c_1 and c_2 and the friction coefficient μ (possibly depending on the vertical load and speed) may be estimated or determined through regression techniques.

1.2.2. Effective Axle Cornering Characteristics

For the basic analysis of (quasi) steady-state turning behaviour a simple two-wheel vehicle model may be used successfully. Effects of suspension and steering system kinematics and compliances such as steer compliance, body roll and also load transfer may be taken into account by using effective axle characteristics. The restriction to (quasi) steady state becomes clear when we realise that for transient or oscillatory motions, exhibiting yaw and roll accelerations and differences in phase, variables like roll angle and load transfer can no longer be written as direct algebraic functions of one of the lateral axle forces (front or rear). Consequently, we should drop the simple method of incorporating the effects of a finite centre of gravity height if the frequency of input signals such as the steering wheel angle cannot be considered small relative to the body roll natural frequency. Since the natural frequency of the wheel suspension and steering systems are relatively high, the restriction to steady-state motions becomes less critical in case of the inclusion of e.g. steering compliance in the effective characteristic. Chiesa and Rinonapoli (1967) were among the first to employ effective axle characteristics or 'working curves' as these were referred to by them. Vågstedt (1995) determined these curves experimentally.

Before assessing the complete non-linear effective axle characteristics we will first direct our attention to the derivation of the effective cornering stiffnesses which are used in the simple linear two-wheel model. For these to be determined, a more comprehensive vehicle model has to be defined.

Figure 1.4 depicts a vehicle model with three degrees of freedom. The forward velocity u may be kept constant. As motion variables we define the lateral velocity v of reference point A, the yaw velocity r and the roll angle φ. A moving axes system (A,x,y,z) has been introduced. The x axis points forwards and lies both in the ground plane and in the plane normal to the ground that passes through the so-called roll axis. The y axis points to the right and the z axis points downwards. This latter axis passes through the centre of gravity when the the roll angle is equal to zero. In this way the location of the point of reference A has been defined. The longitudinal distance to the front axle is a and the distance to the rear axle is b. The sum of the two distances is the wheel base l. For convenience we may write: $a=a_1$ and $b=a_2$.

In a curve, the vehicle body rolls about the roll axis. The location and

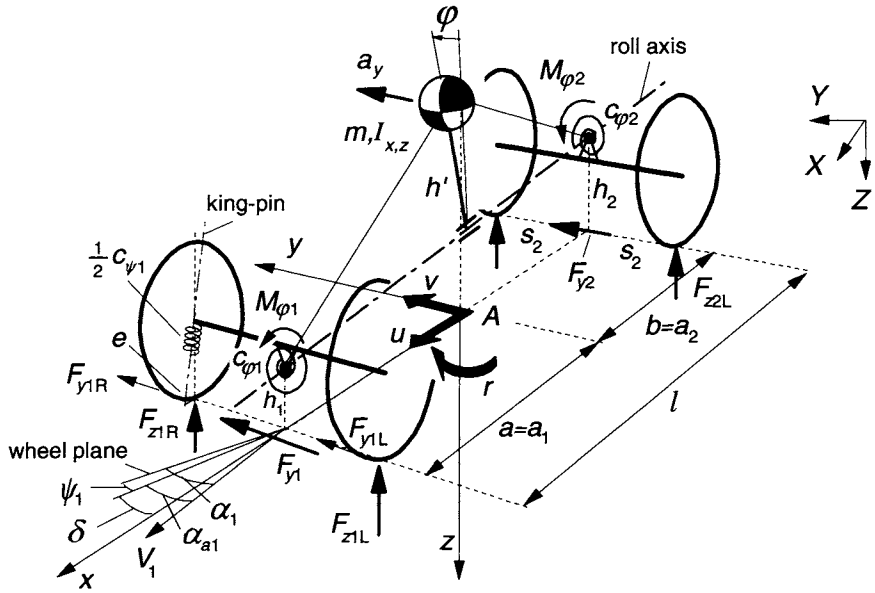

Fig. 1.4. Vehicle model showing three degrees of freedom: lateral, yaw and roll.

attitude of this virtual axis is defined by the heights $h_{1,2}$ of the front and rear roll centres. The roll axis is assessed by considering the body motion with respect to the four contact centres of the wheels on the ground under the action of an external lateral force that acts on the centre of gravity. Due to the symmetry of the vehicle configuration and the linearisation of the model these locations can be considered as fixed. The roll centre locations are governed by suspension kinematics and possibly suspension lateral compliances. The torsional springs depicted in the figure represent the front and rear roll stiffnesses $c_{\varphi 1,2}$ which result from suspension springs and anti-roll bars.

The fore and aft position of the centre of gravity of the body is defined by a and b; its height follows from the distance h' to the roll axis. The body mass is denoted by m and the moments of inertia with respect to the centre of mass and horizontal and vertical axes by I_x, I_z and I_{xz}. These latter quantities will be needed in a later phase when the differential equations of motion are established. The unsprung masses will be neglected or they may be included as point masses attached to the roll axis and thus make them part of the sprung mass, that is, the vehicle body.

Furthermore, the model features torsional springs around the steering axes. The king-pin is positioned at a small caster angle that gives rise to the caster length e as indicated in the drawing. The total steering torsional stiffness, left plus right, is denoted by $c_{\psi 1}$.

Effective Axle Cornering Stiffness

Linear analysis, valid for relatively small levels of lateral accelerations allows the use of approximate tyre characteristics represented by just the slopes at zero slip. We will first derive the effective axle cornering stiffness that may be used under these conditions. The effects of load transfer, body roll, steer compliance, side force steer and initial camber and toe angles will be included in the ultimate expression for the effective axle cornering stiffness.

The linear expressions for the side force and the aligning torque acting on a tyre have been given by Eqs.(1.5). The coefficients appearing in these expressions are functions of the vertical load. For small variations with respect to the average value (designated with subscript o) we write for the cornering and camber force stiffnesses the linearised expressions:

$$\begin{aligned} C_{F\alpha} &= C_{F\alpha o} + \zeta_{\alpha} \Delta F_z \\ C_{F\gamma} &= C_{F\gamma o} + \zeta_{\gamma} \Delta F_z \end{aligned} \tag{1.7}$$

where the increment of the wheel vertical load is denoted by ΔF_z and the slopes of the coefficient versus load curves at $F_z = F_{zo}$ are represented by $\zeta_{\alpha,\gamma}$.

When the vehicle moves steadily around a circular path a centripetal acceleration a_y occurs and a centrifugal force $K = ma_y$ can be said to act on the vehicle body at the centre of gravity in the opposite direction. The body roll angle φ, that is assumed to be small, is calculated by dividing the moment about the roll axis by the apparent roll stiffness which is reduced with the term mgh' due to the additional moment $mgh'\varphi$:

$$\varphi = \frac{-ma_y h'}{c_{\varphi 1} + c_{\varphi 2} - mgh'} \tag{1.8}$$

The total moment about the roll axis is distributed over the front and rear axles in proportion to the front and rear roll stiffnesses. The load transfer ΔF_{zi} from the inner to the outer wheels that occurs at axle i (= 1 or 2) in a steady-state cornering motion with centripetal acceleration a_y follows from the formula:

$$\Delta F_{zi} = \sigma_i m a_y \tag{1.9}$$

with the load transfer coefficient of axle i

$$\sigma_i = \frac{1}{2s_i}\left(\frac{c_{\varphi i}}{c_{\varphi 1} + c_{\varphi 2} - mgh'} h' + \frac{l - a_i}{l} h_i \right) \tag{1.10}$$

The attitude angle of the roll axis with respect to the horizontal is considered small. In the formula, s_i denotes half the track width, h' is the distance from the

centre of gravity to the roll axis and $a_1=a$ and $a_2=b$. The resulting vertical loads at axle i for the left (L) and right (R) wheels become after considering the left and right increments in load:

$$\begin{aligned} \Delta F_{ziL} &= \Delta F_{zi} \quad , \quad \Delta F_{ziR} = -\Delta F_{zi} \\ F_{ziL} &= \tfrac{1}{2} F_{zi} + \Delta F_{zi} \quad , \quad F_{ziR} = \tfrac{1}{2} F_{zi} - \Delta F_{zi} \end{aligned} \tag{1.11}$$

The wheels at the front axle are steered about the king-pins with the angle δ. This angle relates directly to the imposed steering wheel angle δ_{stw} through the steering ratio n_{st}.

$$\delta = \frac{\delta_{stw}}{n_{st}} \tag{1.12}$$

In addition to this imposed steer angle the wheels may show a steer angle and a camber angle induced by body roll through suspension kinematics. The functional relationships with the roll angle may be linearised. For axle i we define:

$$\begin{aligned} \psi_{ri} &= \varepsilon_i \varphi \\ \gamma_{ri} &= \tau_i \varphi \end{aligned} \tag{1.13}$$

Steer compliance gives rise to an additional steer angle due to the external torque that acts about the king-pin (steering axis). For the pair of front wheels this torque results from the side force (of course also from the here not considered driving or braking forces) that exerts a moment about the king-pin through the moment arm which is composed of the caster length e and the pneumatic trail t_1. With the total steering stiffness $c_{\psi 1}$ felt about the king-pins with the steering wheel held fixed, the additional steer angle becomes when for simplicity the influence of camber on the pneumatic trail is disregarded:

$$\psi_{c1} = -\frac{F_{y1}(e + t_1)}{c_{\psi}} \tag{1.14}$$

In addition, the side force (but also the fore and aft force) may induce a steer angle due to suspension compliance. The so-called side force steer reads:

$$\psi_{sfi} = c_{sfi} F_{yi} \tag{1.15}$$

For the front axle, we should separate the influences of moment steer and side force steer. For this reason, side force steer at the front is defined to occur as a result of the side force acting in a point on the king-pin axis.

Beside the wheel angles indicated above, the wheels may have been given initial angles that already exist at straight ahead running. These are the toe angle

ψ_o (positive pointing outwards) and the initial camber angle γ_o (positive: leaning outwards). For the left and right wheels we have the initial angles:

$$\begin{aligned} \psi_{iLo} &= -\psi_{io} \quad , \quad \psi_{iRo} = \psi_{io} \\ \gamma_{iLo} &= -\gamma_{io} \quad , \quad \gamma_{iRo} = \gamma_{io} \end{aligned} \tag{1.16}$$

Adding all relevant contributions (1.12) to (1.16) together yields the total steer angle for each of the wheels.

The effective cornering stiffness of an axle $C_{eff,i}$ is now defined as the ratio of the axle side force and the virtual slip angle. This angle is defined as the angle between the direction of motion of the centre of the axle i (actually at road level) when the vehicle velocity would be very low and approaches zero (then also $F_{yi} \rightarrow 0$) and the direction of motion at the actual speed considered. The virtual slip angle of the front axle has been indicated in Fig.1.4 and is designated as α_{ai}. We have in general:

$$C_{eff,i} = \frac{F_{yi}}{\alpha_{ai}} \tag{1.17}$$

The axle side forces in the steady-state turn can be derived by considering the lateral force and moment equilibrium of the vehicle:

$$F_{yi} = \frac{l - a_i}{l} m a_y \tag{1.18}$$

The axle side force is the sum of the left and right individual tyre side forces. We have

$$\begin{aligned} F_{yiL} &= (\tfrac{1}{2}C_{F\alpha i} + \zeta_{\alpha i}\Delta F_{zi})(\alpha_i - \psi_{io}) + (\tfrac{1}{2}C_{F\gamma i} + \zeta_{\gamma i}\Delta F_{zi})(\gamma_i - \gamma_{io}) \\ F_{yiR} &= (\tfrac{1}{2}C_{F\alpha i} - \zeta_{\alpha i}\Delta F_{zi})(\alpha_i + \psi_{io}) + (\tfrac{1}{2}C_{F\gamma i} - \zeta_{\gamma i}\Delta F_{zi})(\gamma_i + \gamma_{io}) \end{aligned} \tag{1.19}$$

where the average wheel slip angle α_i indicated in the figure is

$$\alpha_i = \alpha_{ai} + \psi_i \tag{1.20}$$

and the average additional steer angle and the average camber angle are:

$$\begin{aligned} \psi_i &= \psi_{ri} + \psi_{ci} + \psi_{sfi} \\ \gamma_i &= \gamma_{ri} \end{aligned} \tag{1.21}$$

The unknown quantity is the virtual slip angle α_{ai} which can be determined for a given lateral acceleration a_y. Next, we use the equations (1.8, 1.9, 1.13, 1.18, 1.14, 1.15), substitute the resulting expressions (1.21) and (1.20) in (1.19) and add up these two equations. The result is a relationship between the axle slip angle α_{ai} and the axle side force F_{yi}. We obtain for the slip angle of axle i:

$$\alpha_{ai} = \frac{F_{yi}}{C_{eff,i}} = \tag{1.22}$$
$$= \frac{F_{yi}}{C_{Fai}}\left(1 + \frac{l(\varepsilon_i C_{Fai} + \tau_i C_{F\gamma i})h'}{(l-a_i)(c_{\varphi 1} + c_{\varphi 2} - mgh')} + \frac{C_{Fai}(e_i + t_i)}{c_{\psi i}} - C_{Fai}c_{sfi} + \frac{2l\sigma_i}{l-a_i}(\zeta_{ai}\psi_{io} + \zeta_{\gamma i}\gamma_{io})\right)$$

The coefficient of F_{yi} constitutes the effective axle cornering compliance, which is the inverse of the effective axle cornering stiffness (1.17). The quantitative effect of each of the suspension, steering and tyre factors included can be easily assessed. The subscript *i* refers to the complete axle. Consequently, the cornering and camber stiffnesses appearing in this expression are the sum of the stiffnesses of the left and right tyre:

$$\begin{aligned} C_{Fai} &= C_{FaiL} + C_{FaiR} = C_{FaiLo} + C_{FaiRo} \\ C_{F\gamma i} &= C_{F\gamma iL} + C_{F\gamma iR} = C_{F\gamma iLo} + C_{F\gamma iRo} \end{aligned} \tag{1.23}$$

in which (1.7) and (1.11) have been taken into account. The load transfer coefficient σ_i follows from Eq.(1.10). Expression (1.22) shows that the influence of lateral load transfer only occurs if initially, at straight ahead running, side forces are already present through the introduction of e.g. opposite steer and camber angles. If these angles are absent, the influence of load transfer is purely non-linear and is only felt at higher levels of lateral accelerations. In the next subsection, this non-linear effect will be incorporated in the effective axle characteristic.

Effective Non-Linear Axle Characteristics

To illustrate the method of effective axle characteristics we will first discuss the determination of the effective characteristic of a front axle showing steering compliance. The steering wheel is held fixed. Due to tyre side forces and self-aligning torques (left and right) distortions will arise resulting in an incremental steer angle ψ_{c1} of the front wheels (ψ_{c1} will be negative in Fig.1.5 for the case of just steer compliance). Since load transfer is not considered in this example, the situation at the left and right wheels are identical (initial toe and camber angles being disregarded). The front tyre slip angle is denoted with α_1. The 'virtual' slip angle of the axle is denoted with α_{a1} and equals (cf. Fig.1.5):

$$\alpha_{a1} = \alpha_1 - \psi_{c1} \tag{1.24}$$

where both α_1 and ψ_{c1} are related with F_{y1} and M_{z1}. The subscipt 1 refers to the front axle and thus to the pair of tyres. Consequently, F_{y1} and M_{z1} denote the sum of the left and right tyre side forces and moments. The objective is, to find the

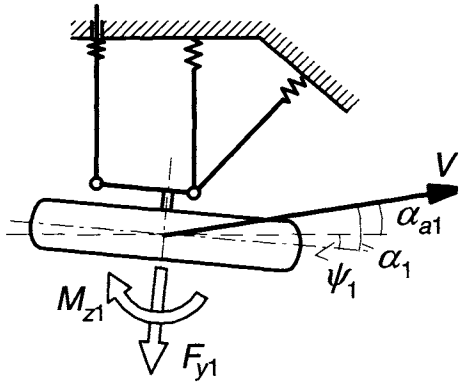

Fig. 1.5. Wheel suspension and steering compliance resulting in additional steer angle ψ_1.

function $F_{y1}(\alpha_{a1})$ which is the effective front axle characteristic. Figure 1.6 shows a graphical approach. According to Eq.(1.24) the points on the $F_{y1}(\alpha_1)$ curve must be shifted horizontally over a length ψ_{c1} to obtain the sought $F_{y1}(\alpha_{a1})$. The slope of the curve at the origin corresponds to the effective axle cornering stiffness found in the preceding subsection. Although the changes with respect to the original characteristic may be small, they can still be of considerable importance since it is the difference of slip angles front and rear which largely determines the vehicle's handling behaviour.

The effective axle characteristic for the case of roll steer can be easily established by subtracting ψ_{ri} from α_i. Instead of using the linear relationships (1.8) and (1.13) non-linear curves may be adopted, possibly obtained from measurements. For the case of roll camber, the situation becomes more complex.

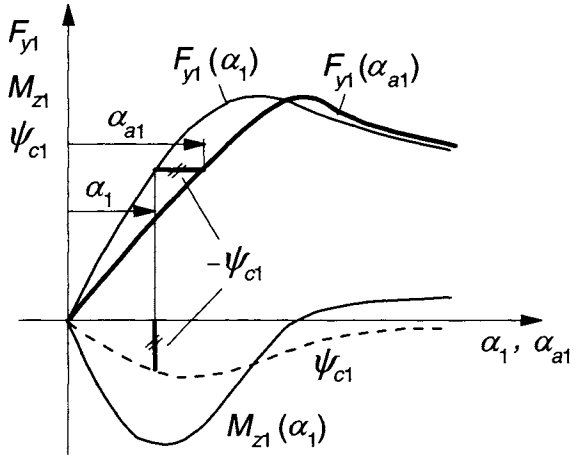

Fig. 1.6. Effective front axle characteristic $F_{y1}(\alpha_{a1})$ influenced by steering compliance.

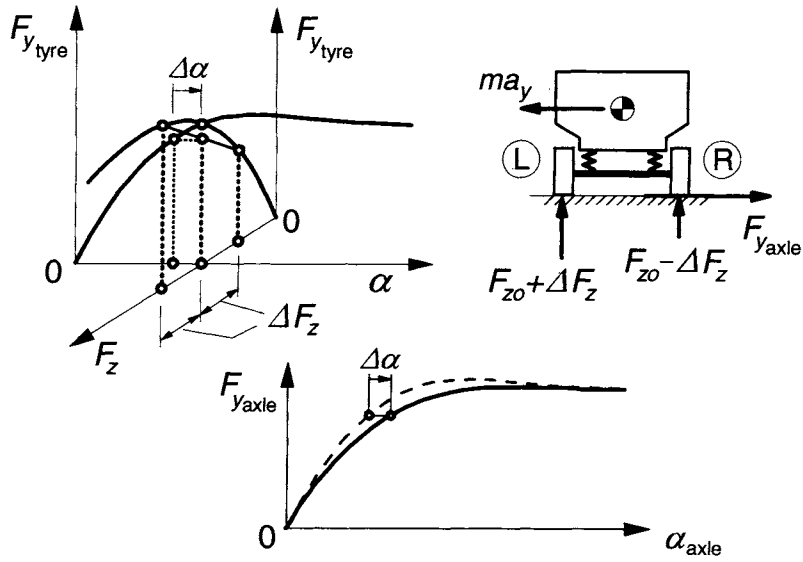

Fig. 1.7. The influence of load transfer on the resulting axle characteristic.

At a given axle side force the roll angle and the associated camber angle can be found. The cornering characteristic of the pair of tyres at that camber angle is needed to find the slip angle belonging to the side force considered.

Load transfer is another example that is less easy to handle. In Fig.1.7 a three dimensional graph is presented for the variation of the side force of an individual tyre as a function of the slip angle and of the vertical load. The former at a given load and the latter at a given slip angle. The diagram illustrates that at load transfer the outer tyre exhibiting a larger load will generate a larger side force than the inner tyre. Because of the non-linear degressive F_y vs F_z curve, however, the average side force will be smaller than the original value it had in the absence of load transfer. The graph indicates that an increase $\Delta\alpha$ of the slip angle would be needed to compensate for the adverse effect of load transfer. The lower diagram gives a typical example of the change in characteristic as a result of load transfer. At the origin the slope is not affected but at larger slip angles an increasingly lower derivative appears to occur. The peak diminishes and may even disappear completely. The way to determine the resulting characteristic is the subject of the next exercise.

Exercise 1.1. Construction of effective axle characteristic at load transfer

For a series of tyre vertical loads F_z the characteristics of the two tyres mounted on, say, the front axle of an automobile are given. In addition, it is known how the load transfer ΔF_z at the front axle depends on the centrifugal force K ($= mg\, F_{y1}/F_{z1} = mg\, F_{y2}/F_{z2}$) acting at the centre of gravity. From this data the resulting cornering charac-

teristic of the axle considered (at steady-state cornering) can be determined.

1. Find the resulting characteristic of one axle from the set of individual tyre characteristics at different tyre loads F_z and the load transfer characteristic both shown in Fig.1.8.
   Hint: First draw in the lower diagram the axle characteristics for values of ΔF_z = 1000, 2000, 3000 and 4000 N and then determine which point on each of these curves is valid considering the load transfer characteristic (left-hand diagram). Draw the resulting axle characteristic.
   It may be helpful to employ the Magic Formula (1.6) and the parameters shown below:
   side force: $F_y = D \sin[C \arctan\{B\alpha - E(B\alpha - \arctan(B\alpha))\}]$
   with factors: $B = C_{F\alpha}/(CD)$, $C = 1.3$, $D = \mu F_z$, $E = -3$, with $\mu = 1$
   cornering stiffness: $C_{F\alpha} = c_1 \sin[2 \arctan\{F_z/c_2\}]$
   with parameters: $c_1 = 60000$ [N/rad], $c_2 = 4000$ [N]
   In addition, we have given for the load transfer: $\Delta F_z = 0.52 F_{y,axle}$ (up to lift-off of the inner tyre, after which the other axle may take over to accommodate the increased total load transfer).
2. Draw the individual curves of F_{yL} and F_{yR} (for the left and right tyre) as a function of α which appear to arise under the load transfer condition considered here.
3. Finally, plot these forces as a function of the vertical load F_z (ranging from 0-8000 N). Note the variation of the lateral force of an individual (left or right) tyre in this same range of vertical load which may be covered in a left and in a right-hand turn at increasing speed of travel until (and possibly beyond) the moment that one of the wheels (the inner wheel) lifts from the ground.

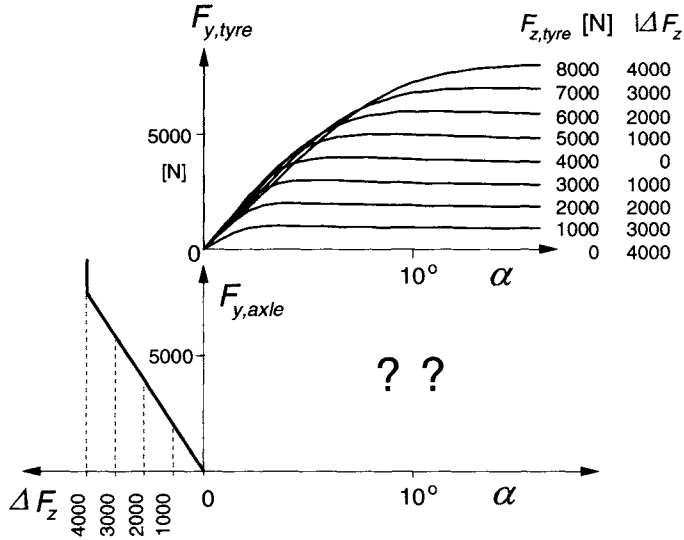

Fig. 1.8. The construction of the resulting axle cornering characteristics at load transfer (Exercise 1.1).

1.3. Vehicle Handling and Stability

In this section attention is paid to the more fundamental aspects of vehicle horizontal motions. Instead of discussing results of computer simulations of complicated vehicle models we rather take the simplest possible model of an automobile that runs at constant speed over an even horizontal road and thereby gain considerable insight into the basic aspects of vehicle handling and stability. Important early work on the linear theory of vehicle handling and stability has been published by Riekert and Schunck (1940), Whitcomb and Milliken (1956) and Segel (1956). Pevsner (1947) studied the non-linear steady-state cornering behaviour at larger lateral accelerations and introduced the handling diagram. One of the first more complete vehicle model studies has been conducted by Pacejka (1958) and by Radt and Pacejka (1963).

For more introductory or specialised study the reader may be referred to books on the subject published earlier, cf. e.g.: Gillespie (1992), Mitschke (1990), Milliken and Milliken (1995) and Kortüm and Lugner (1994).

The derivation of the equations of motion for the three degree of freedom model of Fig.1.4 will be treated first after which the simple model with two degrees of freedom is considered and analysed. This analysis comprises the steady-state response to steering input and the stability of the resulting motion. Also, the frequency response to steering fluctuations and external disturbances will be discussed, first for the linear vehicle model and subsequently for the non-linear model where large lateral accelerations and disturbances are introduced.

The simple model to be employed in the analysis is presented in Fig.1.9. The track width has been neglected with respect to the radius of the cornering motion

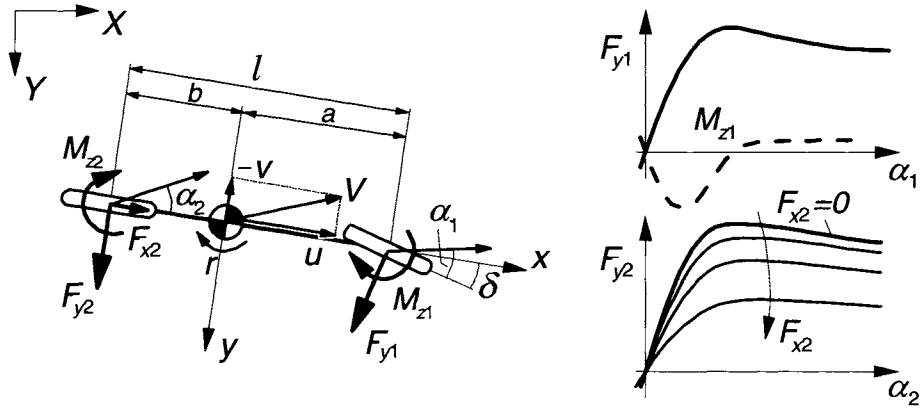

Fig. 1.9. Simple car model with side force characteristics for front and rear (driven) axle.

which allows the use of a two-wheel vehicle model. The steer and slip angles will be restricted to relatively small values. Then, the variation of the geometry may be regarded to remain linear, that is: $\cos\alpha \approx 1$ and $\sin\alpha \approx \alpha$ and similarly for the steer angle δ. Moreover, the driving force required to keep the speed constant is assumed to remain small with respect to the lateral tyre force. Considering combined slip curves like those shown in Fig.1.2 (right), we may draw the conclusion that the influence of F_x on F_y may be neglected in that case.

In principle, a model as shown in Fig.1.9 lacks body roll and load transfer. Therefore, the theory is actually limited to cases where the roll moment remains small, that is at low friction between tyre and road or a low centre of gravity relative to the track width. This restriction may be overcome by using the effective axle characteristics in which the effects of body roll and load transfer have been included while still adhering to the simple (rigid) two-wheel vehicle model. As has been mentioned before, this is only permissible when the frequency of the imposed steer angle variations remains small with respect to the roll natural frequency. Similarly, as has been demonstrated in the preceding section, effects of other factors like compliance in the steering system and suspension mounts may be accounted for.

The speed of travel is considered to be constant. However, the theory may approximately hold also for quasi-steady-state situations for instance at moderate braking or driving. The influence of the fore-and-aft force F_x on the tyre or axle cornering force vs slip angle characteristic (F_y, α) may then be regarded (cf. Fig.1.9). The forces F_{y1} and F_{x1} and the moment M_{z1} are defined to act upon the single front wheel and similarly we define F_{y2} etc. for the rear wheel.

1.3.1. Differential Equations for Plane Vehicle Motions

In this section, the differential equations for the three degree of freedom vehicle model of Fig.1.4 will be derived. In first instance, the fore and aft motion will also be left free to vary. The resulting set of equations of motion may be of interest for the reader to further study the vehicle's dynamic response at somewhat higher frequencies where the roll dynamics of the vehicle body may become of importance. From these equations, the equations for the simple two-degree of freedom model of Fig.1.9 used in the subsequent section can be easily assessed. In Subsection 1.3.6 the equations for the car with trailer will be established. The possible instability of the motion will be studied.

We will employ Lagrange's equations to derive the equations of motion. For a system with n degrees of freedom n (generalised) coordinates q_i are selected which are sufficient to completely describe the motion while possible kinematic

constraints remain satisfied. The moving system possesses kinetic energy T and potential energy U. External generalised forces Q_i associated with the generalised coordinates q_i may act on the system and do work W. Internal forces acting from dampers to the system structure may be regarded as external forces taking part in the total work W. The equation of Lagrange for coordinate q_i reads:

$$\frac{d}{dt}\frac{\partial T}{\partial \dot{q}_i} - \frac{\partial T}{\partial q_i} + \frac{\partial U}{\partial q_i} = Q_i \tag{1.25}$$

The system depicted in Fig.1.4 and described in the preceding subsection performs a motion over a flat level road. Proper coordinates are the Cartesian coordinates X and Y of reference point A, the yaw angle ψ of the moving x axis with respect to the inertial X axis and finally the roll angle φ about the roll axis. For motions near the X axis and thus small yaw angles, Eq.(1.25) is adequate to derive the equations of motion. For cases where ψ may attain large values, e.g. when moving along a circular path, it is preferred to use modified equations where the velocities u, v and r of the moving axes system are used as generalised motion variables in addition to the coordinate φ. The relations between the two sets of variables are (the dots referring to differentiation with respect to time):

$$\begin{aligned} u &= \dot{X}\cos\psi + \dot{Y}\sin\psi \\ v &= -\dot{X}\sin\psi + \dot{Y}\cos\psi \\ r &= \dot{\psi} \end{aligned} \tag{1.26}$$

The kinetic energy can be expressed in terms of u, v and r. Preparation of the first terms of Eq.(1.25) for the coordinates X, Y and ψ yields:

$$\begin{aligned} \frac{\partial T}{\partial \dot{X}} &= \frac{\partial T}{\partial u}\frac{\partial u}{\partial \dot{X}} + \frac{\partial T}{\partial v}\frac{\partial v}{\partial \dot{X}} = \frac{\partial T}{\partial u}\cos\psi - \frac{\partial T}{\partial v}\sin\psi \\ \frac{\partial T}{\partial \dot{Y}} &= \frac{\partial T}{\partial u}\frac{\partial u}{\partial \dot{Y}} + \frac{\partial T}{\partial v}\frac{\partial v}{\partial \dot{Y}} = \frac{\partial T}{\partial u}\sin\psi + \frac{\partial T}{\partial v}\cos\psi \\ \frac{\partial T}{\partial \dot{\psi}} &= \frac{\partial T}{\partial r} \\ \frac{\partial T}{\partial \psi} &= \frac{\partial T}{\partial u}v - \frac{\partial T}{\partial v}u \end{aligned} \tag{1.27}$$

The yaw angle ψ may now be eliminated by multiplying the final equations for X and Y successively with $\cos\psi$ and $\sin\psi$ and subsequently adding and subtracting them. The resulting equations represent the equilibrium in the x and y (or u and v) directions respectively.

We obtain the following set of modified Lagrangean equations for the first three variables u, v and r and subsequently for the remaining real coordinates

(for our system only φ) :

$$\begin{aligned}
&\frac{d}{dt}\frac{\partial T}{\partial u} - r\frac{\partial T}{\partial v} = Q_u \\
&\frac{d}{dt}\frac{\partial T}{\partial v} + r\frac{\partial T}{\partial u} = Q_v \\
&\frac{d}{dt}\frac{\partial T}{\partial r} - v\frac{\partial T}{\partial u} + u\frac{\partial T}{\partial v} = Q_r \\
&\frac{d}{dt}\frac{\partial T}{\partial \dot{\varphi}} - \frac{\partial T}{\partial \varphi} + \frac{\partial U}{\partial \varphi} = Q_\varphi
\end{aligned} \tag{1.28}$$

The generalised forces are found from the virtual work:

$$\delta W = \sum_{j=1}^{4} Q_j \delta q_j \tag{1.29}$$

with q_j referring to the quasi coordinates x and y and the coordinates ψ and φ. Note that x and y can not be found from integrating u and v. For that reason the term 'quasi' coordinate is used. For the vehicle model we find for the virtual work as a result of the virtual displacements δx, δy, $\delta\psi$ and $\delta\varphi$:

$$\delta W = \sum F_x \delta x + \sum F_y \delta y + \sum M_z \delta\psi + \sum M_\varphi \delta\varphi \tag{1.30}$$

where apparently

$$\begin{aligned}
Q_u &= \sum F_x = F_{x1}\cos\delta - F_{y1}\sin\delta + F_{x2} \\
Q_v &= \sum F_y = F_{x1}\sin\delta + F_{y1}\cos\delta + F_{y2} \\
Q_r &= \sum M_z = aF_{x1}\sin\delta + aF_{y1}\cos\delta + M_{z1} - bF_{y2} + M_{z2} \\
Q_\varphi &= \sum M_\varphi = -(k_{\varphi 1} + k_{\varphi 2})\dot{\varphi}
\end{aligned} \tag{1.31}$$

The longitudinal forces are assumed to be the same at the left and right wheels and the effect of additional steer angles ψ_i are neglected here. Shock absorbers in the wheel suspensions are represented by the resulting linear moments about the roll axes with damping coefficients $k_{\varphi i}$ at the front and rear axles.

With the roll angle φ and the roll axis inclination angle $\theta_r \approx (h_2 - h_1)/l$ assumed small, the kinetic energy becomes:

$$\begin{aligned}
T = {}&\tfrac{1}{2}m\{(u - h'\varphi r)^2 + (v + h'\dot{\varphi})^2\} + \\
&+\tfrac{1}{2}I_x\dot{\varphi}^2 + \tfrac{1}{2}I_y(\varphi r)^2 + \tfrac{1}{2}I_z(r^2 - \varphi^2 r^2 + 2\theta_r r\dot{\varphi}) - I_{xz}r\dot{\varphi}
\end{aligned} \tag{1.32}$$

The potential energy U is built up in the suspension springs (including the radial tyre compliances) and through the height of the centre of gravity. We have, again for small angles:

$$U = \tfrac{1}{2}(c_{\varphi 1} + c_{\varphi 2})\varphi^2 - \tfrac{1}{2}mgh'\varphi^2 \tag{1.33}$$

The equations of motion are finally established by using the expressions (1.31), (1.32) and (1.33) in the equations (1.28). The equations will be linearised in the assumedly small angles φ and δ. For the variables u, v, r and φ we obtain successively:

$$m(\dot{u} - rv - h'\varphi\dot{r} - 2h'r\dot{\varphi}) = F_{x1} - F_{y1}\delta + F_{x2} \tag{1.34a}$$

$$m(\dot{v} + ru + h'\ddot{\varphi} - h'r^2\varphi) = F_{x1}\delta + F_{y1} + F_{y2} \tag{1.34b}$$

$$I_z\dot{r} + (I_z\theta_r - I_{xz})\ddot{\varphi} - mh'(\dot{u} - rv)\varphi = aF_{x1}\delta + aF_{y1} + M_{z1} - bF_{y2} + M_{z2} \tag{1.34c}$$

$$(I_x + mh'^2)\ddot{\varphi} + mh'(\dot{v} + ru) + (I_z\theta_r - I_{xz})\dot{r} - (mh'^2 + I_y - I_z)r^2\varphi + \\ + (k_{\varphi 1} + k_{\varphi 2})\dot{\varphi} + (c_{\varphi 1} + c_{\varphi 2} - mgh')\varphi = 0 \tag{1.34d}$$

Note that the small additional roll and compliance steer angles ψ_i have been neglected in the assessment of the force components. The tyre side forces depend on the slip and camber angles front and rear and on the tyre vertical loads. We may need to take the effect of combined slip into account. The longitudinal forces are either given as a result of brake effort or imposed propulsion torque or they depend on the wheel longitudinal slip which follows from the wheel speed of revolution requiring four additional wheel rotational degrees of freedom. The first equation (1.34a) may be used to compute the propulsion force needed to keep the forward speed constant.

The vertical loads and more specifically the load transfer can be obtained by considering the moment equilibrium of the front and rear axle about the respective roll centres. For this, the roll moments $M_{\varphi i}$ (cf. Fig.1.4) resulting from suspension springs and dampers as appear in Eq.(1.34d) through the terms with subscript 1 and 2 respectively, and the axle side forces appearing in Eq.(1.34b) are to be regarded. For a linear model the load transfer can be neglected if initial (left/right opposite) wheel angles are disregarded. We have at steady-state (effect of damping vanishes):

$$\Delta F_{zi} = \frac{-c_{\varphi i}\varphi + F_{yi}h_i}{2s_i} \tag{1.35}$$

The front and rear slip angles follow from the lateral velocities of the wheel axles and the wheel steer angles with respect to the moving longitudinal x axis. The longitudinal velocities of the wheel axles may be regarded the same left and right

and equal to the vehicle longitudinal speed u. This is allowed when $s_i|r| \ll u$. Then the expressions for the assumedly small slip angles read:

$$\alpha_1 = \delta + \psi_1 - \frac{v + ar - e\dot{\delta}}{u}$$
$$\alpha_2 = \psi_2 - \frac{v - br}{u} \tag{1.36}$$

The additional roll and compliance steer angles ψ_i and the wheel camber angles γ_i are obtained from Eq.(1.21) with (1.13-15) or corresponding non-linear expressions. Initial wheel angles are assumed to be equal to zero. The influence of the steer angle velocity appearing in the expression for the front slip angle is relatively small and may be disregarded. The small products of the caster length e and the time rate of change of ψ_i have been neglected in the above expressions.

Equations (1.34) may be further linearised by assuming that all the deviations from the rectilinear motion are small. This allows the neglection of all products of variable quantities which vanish when the vehicle moves straight ahead. The side forces and moments are then written as in Eq.(1.5) with the subscripts $i=1$ or 2 provided. If the moment due to camber is neglected and the pneumatic trail is introduced in the aligning torque we have:

$$F_{yi} = F_{y\alpha i} + F_{y\gamma i} = C_{F\alpha i}\alpha_i + C_{F\gamma i}\gamma_i$$
$$M_{zi} = M_{z\alpha i} = -C_{M\alpha i}\alpha_i = -t_i F_{y\alpha i} = -t_i C_{F\alpha i}\alpha_i \tag{1.37}$$

The three linear equations of motion for the system of Fig.1.4 with the forward speed u kept constant finally turn out to read expressed solely in terms of the three motion variables v, r and φ:

$$m(\dot{v} + ur + h'\ddot{\varphi}) = C_{F\alpha 1}\{(1 + c_{sc1})(u\delta + e\dot{\delta} - v - ar)/u + c_{sr1}\varphi\} + \\ + C_{F\alpha 2}\{(1 + c_{sc2})(-v + br)/u + c_{sr2}\varphi\} + (C_{F\gamma 1}\tau_1 + C_{F\gamma 2}\tau_2)\varphi \tag{1.38a}$$

$$I_z\dot{r} + (I_z\theta_r - I_{xz})\ddot{\varphi} = (a - t_1)C_{F\alpha 1}\{(1 + c_{sc1})(u\delta + e\dot{\delta} - v - ar)/u + c_{sr1}\varphi\} + \\ - (b + t_2)C_{F\alpha 2}\{(1 + c_{sc2})(-v + br)/u + c_{sr2}\varphi\} + (aC_{F\gamma 1}\tau_1 - bC_{F\gamma 2}\tau_2)\varphi \tag{1.38b}$$

$$(I_x + mh'^2)\ddot{\varphi} + mh'(\dot{v} + ur) + (I_z\theta_r - I_{xz})\dot{r} + (k_{\varphi 1} + k_{\varphi 2})\dot{\varphi} + \\ + (c_{\varphi 1} + c_{\varphi 2} - mgh')\varphi = 0 \tag{1.38c}$$

In these equations the additional steer angles ψ_i have been eliminated by using expressions (1.21) with (1.13-15). Furthermore, the resulting compliance steer

and roll steer coefficients for $i = 1$ or 2 have been introduced:

$$c_{sci} = \frac{\left(c_{sfi} - \dfrac{e_i + t_i}{c_{\psi i}}\right) C_{F\alpha i}}{1 - \left(c_{sfi} - \dfrac{e_i + t_i}{c_{\psi i}}\right) C_{F\alpha i}}, \quad c_{sri} = \frac{\varepsilon_i + \tau_i \left(c_{sfi} - \dfrac{e_i + t_i}{c_{\psi i}}\right) C_{F\gamma i}}{1 - \left(c_{sfi} - \dfrac{e_i + t_i}{c_{\psi i}}\right) C_{F\alpha i}} \tag{1.39}$$

where the steer stiffness at the rear $c_{\psi 2}$ may be taken equal to infinity. Furthermore, we have the roll axis inclination angle:

$$\theta_r = \frac{h_2 - h_1}{l} \tag{1.40}$$

In Chapters 7 and 8 the transient properties of the tyre will be addressed. The relaxation length denoted by σ_i is an important parameter that controls the lag of the response of the side force to the input slip angle. For the Laplace transformed version of the equations (1.38) with the Laplace variable s representing differentiation with respect to time, we may introduce tyre lag by replacing the slip angle α_i by the filtered transient slip angle. This may be accomplished by replacing the cornering stiffnesses $C_{F\alpha i}$ appearing in (1.38) and (1.39) by the 'transient stiffnesses':

$$C_{F\alpha i} \rightarrow \frac{C_{F\alpha i}}{1 + s\sigma_i / u} \tag{1.41}$$

A similar procedure may be followed to include the tyre transient response to wheel camber variations. The relaxation length concerned is about equal to the one used for the response to side slip variations. At nominal vertical load the relaxation length is of the order of magnitude of the wheel radius. A more precise model of the aligning torque may be introduced by using a transient pneumatic trail with a similar replacement as indicated by (1.41) but with a much smaller relaxation length approximately equal to half the contact length of the tyre. For more details we refer to Chapter 9 that is dedicated to short wavelength force and moment response.

1.3.2. Linear Analysis of the Two-Degree of Freedom Model

From the equations (1.34b and c) the reduced set of equations for the two-degree of freedom model can be derived immediately. The roll angle φ and its derivative are set equal to zero and furthermore, we will assume the forward speed u ($\approx V$) to remain constant and neglect the influence of the lateral component of the longitudinal forces F_{xi}. The equations of motion of the simple model of Fig.1.9 for v and r now read:

$$m(\dot{v} + ur) = F_{y1} + F_{y2} \tag{1.42a}$$

$$I\dot{r} = aF_{y1} - bF_{y2} \tag{1.42b}$$

with v denoting the lateral velocity of the centre of gravity and r the yaw velocity. The symbol m stands for the vehicle mass and I ($=I_z$) denotes the moment of inertia about the vertical axis through the centre of gravity. For the matter of simplicity, the rearward shifts of the points of application of the forces F_{y1} and F_{y2} over a length equal to the pneumatic trail t_1 and t_2 respectively (that is the aligning torques) have been disregarded. Later, we come back to this. The side forces are functions of the respective slip angles:

$$F_{y1} = F_{y1}(\alpha_1) \quad \text{and} \quad F_{y2} = F_{y2}(\alpha_2) \tag{1.43}$$

and the slip angles are expressed by

$$\alpha_1 = \delta - \frac{1}{u}(v + ar) \quad \text{and} \quad \alpha_2 = -\frac{1}{u}(v - br) \tag{1.44}$$

neglecting the effect of the time rate of change of the steer angle appearing in Eq.(1.36). For relatively low frequency motions the effective axle characteristics or effective cornering stiffnesses according to Eqs.(1.17, 1.22) may be employed.

When only small deviations with respect to the undisturbed straight-ahead motion are considered, the slip angles may be assumed to remain small enough to allow linearisation of the cornering characteristics. For the side force the relationship with the slip angle reduces to the linear equation:

$$F_{yi} = C_i\alpha_i = C_{Fai}\alpha_i \tag{1.45}$$

where C_i denotes the cornering stiffness. This can be replaced by the symbol C_{Fai} which may be preferred in more general cases where also camber and aligning stiffnesses play a role.

The two linear first-order differential equations now read:

$$\begin{aligned} m\dot{v} + \frac{1}{u}(C_1 + C_2)v + \left\{mu + \frac{1}{u}(aC_1 - bC_2)\right\}r &= C_1\delta \\ I\dot{r} + \frac{1}{u}(a^2C_1 + b^2C_2)r + \frac{1}{u}(aC_1 - bC_2)v &= aC_1\delta \end{aligned} \tag{1.46}$$

After elimination of the lateral velocity v we obtain the second-order differential equation for the yaw rate r:

$$\begin{aligned} Imu\ddot{r} + \{I(C_1 + C_2) + m(a^2C_1 + b^2C_2)\}\dot{r} + \\ + \frac{1}{u}\{C_1C_2l^2 - mu^2(aC_1 - bC_2)\}r = muaC_1\dot{\delta} + C_1C_2l\delta \end{aligned} \tag{1.47}$$

Here, as before, the dots refer to differentiation with respect to time, δ is the steer angle of the front wheel and l $(=a+b)$ represents the wheel base. The equations may be simplified by introducing the following quantities:

$$\begin{aligned} C &= C_1 + C_2 \\ Cs &= C_1a - C_2b \\ Cq^2 &= C_1a^2 + C_2b^2 \\ mk^2 &= I \end{aligned} \tag{1.48}$$

Here, C denotes the total cornering stiffness of the vehicle, s is the distance from the centre of gravity to the so-called neutral steer point S (Fig. 1.11), q is a length corresponding to an average moment arm and k is the radius of gyration. Equations (1.46) and (1.47) now reduce to:

$$\begin{aligned} m(\dot{v} + ur) + \frac{C}{u}v + \frac{Cs}{u}r &= C_1\delta \\ mk^2\dot{r} + \frac{cq^2}{u}r + \frac{Cs}{u}v &= C_1a\delta \end{aligned} \tag{1.49}$$

and with v eliminated:

$$m^2k^2u^2\ddot{r} + mC(q^2 + k^2)u\dot{r} + (C_1C_2l^2 - mu^2Cs)r = mu^2aC_1\dot{\delta} + uC_1C_2l\delta \tag{1.50}$$

The neutral steer point S is defined as the point on the longitudinal axis of the vehicle where an external side force can be applied without changing the vehicle's yaw angle. If the force acts in front of the neutral steer point, the vehicle is expected to yaw in the direction of the force; if behind, then against the force. The point is of interest when discussing the steering characteristics and stability.

Linear Steady-State Cornering Solutions

We are interested in the path curvature ($1/R$) that results from a constant steer angle δ at a given constant speed of travel V. Since we have at steady state:

$$\frac{1}{R} = \frac{r}{V} \approx \frac{r}{u} \tag{1.51}$$

the expression for the path curvature becomes using (1.47) with u replaced by V and the time derivatives omitted:

$$\frac{1}{R} = \frac{C_1 C_2 l}{C_1 C_2 l^2 - m V^2 (a C_1 - b C_2)} \delta \tag{1.52}$$

By taking the inverse, the expression for the steer angle required to negotiate a curve with a given radius R is obtained:

$$\delta = \frac{1}{R}\left(l - m V^2 \frac{a C_1 - b C_2}{l C_1 C_2} \right) \tag{1.53}$$

It is convenient to introduce the so-called understeer coefficient or gradient η. For our model, this quantity is defined as

$$\eta = -\frac{mg}{l} \frac{a C_1 - b C_2}{C_1 C_2} = -\frac{s}{l} \frac{mgC}{C_1 C_2} \tag{1.54}$$

with g denoting the acceleration due to gravity. After having defined the lateral acceleration which in the present linear analysis equals the centripetal acceleration:

$$a_y = Vr = \frac{V^2}{R} \tag{1.55}$$

Eq.(1.53) can be written in the more convenient form

$$\delta = \frac{l}{R}\left(1 + \eta \frac{V^2}{gl} \right) = \frac{l}{R} + \eta \frac{a_y}{g} \tag{1.56}$$

The meaning of understeer versus oversteer becomes clear when the steer angle is plotted against the centripetal acceleration while the radius R is kept constant. In Fig.1.10 (left-hand diagram) this is done for three types of vehicles showing understeer, neutral steer and oversteer. Apparently, for an understeered vehicle, the steer angle needs to be increased when the vehicle is going to run at a higher speed. At neutral steer the steer angle can be kept constant while at oversteer a reduction in steer angle is needed when the speed of travel is increased and at the same time a constant turning radius is maintained.

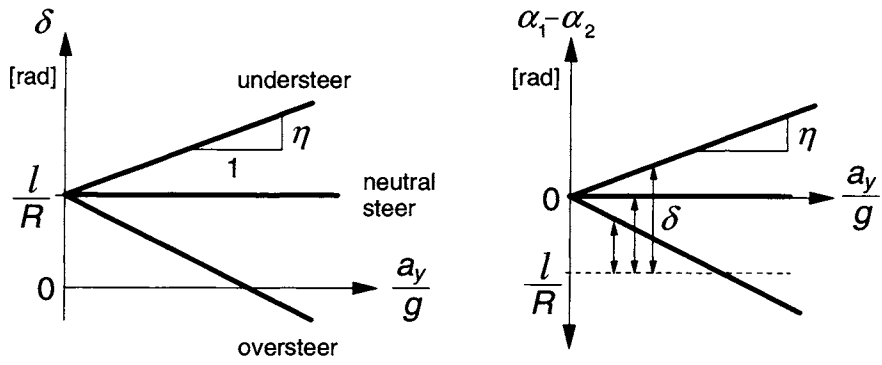

Fig. 1.10. The steer angle versus lateral acceleration at constant path curvature (left graph). The difference in slip angle versus lateral acceleration and the required steer angle at a given path curvature (right graph). The understeer gradient η.

According to Eq.(1.56) the steer angle changes sign when for an oversteered car the speed increases beyond the critical speed that is expressed by:

$$V_{crit} = \sqrt{\frac{g\,l}{-\eta}} \qquad (\eta < 0) \tag{1.57}$$

As will be shown later, the motion becomes unstable when the critical speed is surpassed. Apparently, this can only happen when the vehicle shows oversteer.

For an understeered car a counterpart has been defined which is the so-called characteristic speed. It is the speed where the steer angle required to maintain the same curvature increases to twice the angle needed at speeds approaching zero. We may also say that at the characteristic speed the path curvature response to steer angle has decreased to half its value at very low speed. Also interesting is the fact that at the characteristic speed the yaw rate response to steer angle r/δ reaches a maximum (the proof of which is left to the reader). We have for the characteristic velocity:

$$V_{char} = \sqrt{\frac{g\,l}{\eta}} \qquad (\eta > 0) \tag{1.58}$$

Expression (1.54) for the understeer gradient η is simplified when the following expressions for the front and rear axle loads are used:

$$F_{z1} = \frac{b}{l} m g \quad \text{and} \quad F_{z2} = \frac{a}{l} m g \tag{1.59}$$

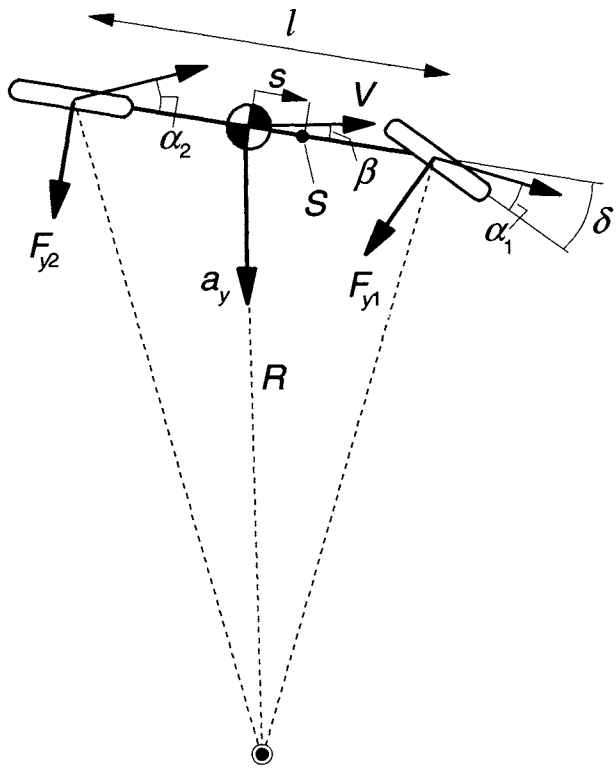

Fig. 1.11. Two-wheel vehicle model in a cornering manoeuvre.

We obtain:

$$\eta = \frac{F_{z1}}{C_1} - \frac{F_{z2}}{C_2} \tag{1.60}$$

which says that a vehicle exhibits an understeer nature when the relative cornering compliance of the tyres at the front is larger than at the rear. It is important to note that in (1.59) and (1.60) the quantities $F_{z1,2}$ denote the vertical axle loads that occur at stand-still and thus represent the mass distribution of the vehicle. Changes of these loads due to aerodynamic down forces and fore and aft load transfer at braking or driving should not be introduced in expression (1.60).

In the same diagram the difference in slip angle front and rear may be indicated. We find for the side forces

$$F_{y1} = \frac{b}{l} m a_y = F_{z1} \frac{a_y}{g}, \qquad F_{y2} = \frac{a}{l} m a_y = F_{z2} \frac{a_y}{g} \tag{1.61}$$

and hence for the slip angles

$$\alpha_1 = \frac{F_{z1}}{C_1}\frac{a_y}{g}, \qquad \alpha_2 = \frac{F_{z2}}{C_2}\frac{a_y}{g} \tag{1.62}$$

The difference now reads when considering the relation (1.59)

$$\alpha_1 - \alpha_2 = \eta \frac{a_y}{g} \tag{1.63}$$

Apparently, the sign of this difference is dictated by the understeer coefficient. Consequently, it may be stated that according to the linear model an understeered vehicle ($\eta > 0$) moves in a curve with slip angles larger at the front than at the rear ($\alpha_1 > \alpha_2$). For a neutrally steered vehicle the angles remain the same ($\alpha_1 = \alpha_2$) and with an oversteered car the rear slip angles are bigger ($\alpha_2 > \alpha_1$). As is shown by the expressions (1.54), the signs of η and s are different. Consequently, as one might expect when the centrifugal force is considered as the external force, a vehicle acts oversteered when the neutral steer point lies in front of the centre of gravity and understeered when S lies behind the c.g.. As we will see later on, the actual non-linear vehicle may change its steering character when the lateral acceleration increases. It appears then that the difference in slip angle is no longer directly related to the understeer gradient.

Consideration of Eq.(1.56) reveals that in the left-hand graph of Fig.1.10 the difference in slip angle can be measured along the ordinate starting from the value l/R. It is of interest to convert the diagram into the graph shown on the right-hand side of Fig.1.10 with ordinate equal to the difference in slip angle. In that way, the diagram becomes more flexible because the value of the curvature $1/R$ may be selected afterwards. The horizontal dotted line is then shifted vertically according to the value of the relative curvature l/R considered. The distance to the handling line represents the magnitude of the steer angle.

Figure 1.11 depicts the resulting steady-state cornering motion. The vehicle side slip angle β has been indicated. It is of interest to note that at low speed this angle is negative for right-hand turns. Beyond a certain value of speed the tyre slip angles have become sufficiently large and the vehicle slip angle changes into positive values. In Exercise 1.2 the slip angle β will be used.

Influence of the Pneumatic Trail

The direct influence of the pneumatic trails t_i may not be negligible. In reality, the tyre side forces act a small distance behind the contact centres. As a consequence, the neutral steer point should also be considered to be located at a distance approximately equal to the average value of the pneumatic trails, more

to the rear, which means actually more understeer. The correct values of the position s of the neutral steer point and of the understeer coefficient η can be found by using the effective axle distances $a' = a - t_1$, $b' = b + t_2$ and $l' = a' + b'$ in the Eqs.(1.48) and (1.59) instead of the original quantities a, b and l.

Stability of the Motion

Stability of the steady-state circular motion can be examined by considering the differential equation (1.47) or (1.50). The steer angle is kept constant so that the equation gets the form

$$a_0 \ddot{r} + a_1 \dot{r} + a_2 r = b_1 \delta \tag{1.64}$$

For this second-order differential equation stability is assured when all coefficients a_i are positive. Only the last coefficient a_2 may become negative which corresponds to divergent instability (spin-out without oscillations). As already indicated, this will indeed occur when for an oversteered vehicle the critical speed (1.57) is exceeded. The condition for stability reads:

$$a_2 = C_1 C_2 l^2 \left(1 + \eta \frac{V^2}{g\,l} \right) = C_1 C_2 l^2 \left(\frac{\delta}{l/R} \right)_{ss} > 0 \tag{1.65}$$

with the subscript ss referring to steady-state conditions, or

$$V < V_{crit} = \sqrt{\frac{g\,l}{-\eta}} \qquad (\eta < 0) \tag{1.66}$$

The next section will further analyse the dynamic nature of the stable and unstable motions.

It is of importance to note that when the condition of an automobile subjected to driving or braking forces is considered, the cornering stiffnesses front and rear will change due to the associated fore and aft axle load transfer and the resulting state of combined slip. In expression (1.60) for the understeer coefficient η the quantities F_{zi} represent the static vertical axle loads obtained through Eqs.(1.59) and are to remain unchanged! In Subsection 1.3.4 the effect of longitudinal forces on vehicle stability will be further analysed.

Free Linear Motions

To study the nature of the free motion after a small disturbance in terms of natural frequency and damping, the eigenvalues, that is the roots of the characteristic equation of the linear second-order system, are to be assessed. The

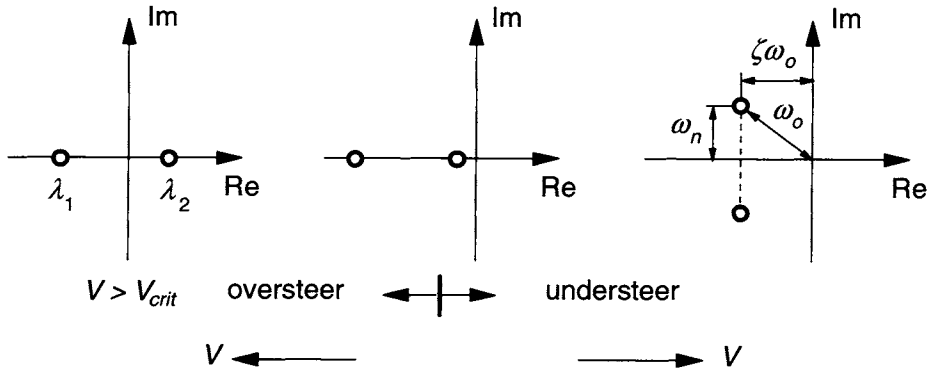

Fig. 1.12. Possible eigenvalues for the over and understeered car at lower and higher speeds.

characteristic equation of the system described by the equations (1.49) or (1.50) reads after using the relation (1.54) between s and η:

$$m^2k^2V^2\lambda^2 + mC(q^2 + k^2)V\lambda + C_1C_2l^2\left(1 + \frac{\eta}{gl}V^2\right) = 0 \qquad (1.67)$$

For a single mass-damper-spring system shown in Fig.1.13 with r the mass displacement, δ the forced displacement of the support, M the mass, D the sum of the two damping coefficients D_1 and D_2 and K the sum of the two spring stiffnesses K_1 and K_2 a differential equation similar in structure to Eq.(1.50) arises:

$$M\ddot{r} + D\dot{r} + Kr = D_1\dot{\delta} + K_1\delta \qquad (1.68)$$

and the corresponding characteristic equation:

$$M\lambda^2 + D\lambda + K = 0 \qquad (1.69)$$

When an oversteered car exceeds its critical speed, the last term of (1.67) becomes negative which apparently corresponds with a negative stiffness K. An inverted pendulum is an example of a second-order system with negative last coefficient showing monotonous (diverging) instability.

The roots λ of equation (1.67) may have loci in the complex plane as shown in Fig.1.12. For positive values of the cornering stiffnesses only the last coefficient of the characteristic equation can become negative which is responsible for the limited types of eigenvalues that can occur. As we will see in Subsection 1.3.3, possible negative slopes beyond the peak of the non-linear axle characteristics may give rise to other types of unstable motions connected with two positive real roots or two conjugated complex roots with a positive real part. For the linear vehicle model we may have two real roots in the oversteer case and

a pair of complex roots in the understeer case, except at low speeds where the understeered vehicle can show a pair of real negative roots.

As indicated in the figure, the complex root is characterised by the natural frequency ω_0 of the undamped system ($D = 0$), the damping ratio ζ and the resulting actual natural frequency ω_n. Expressions for these quantities in terms of the model parameters are rather complex. However, if we take into account that in normal cases $|s| \ll l$ and $q \approx k \approx \frac{1}{2} l$ we may simplify these expressions and find the following useful formulae:

The natural frequency of the undamped system:

$$\omega_o^2 = \frac{K}{M} \approx \left(\frac{C}{mV}\right)^2 \cdot \left(1 + \frac{\eta}{gl} V^2\right) \tag{1.70}$$

The damping ratio:

$$\zeta = \frac{D}{2M\omega_o} \approx \frac{1}{\sqrt{1 + \frac{\eta}{gl} V^2}} \tag{1.71}$$

The natural frequency:

$$\omega_n^2 = \omega_o^2 (1 - \zeta^2) \approx \left(\frac{C}{m}\right)^2 \frac{\eta}{gl} \tag{1.72}$$

The influence of parameters has been indicated in Fig.1.13. An arrow pointing upwards represents an increase of the quantity in the same column of the matrix.

The yaw rate response to a step change in steer angle is typified by the rise

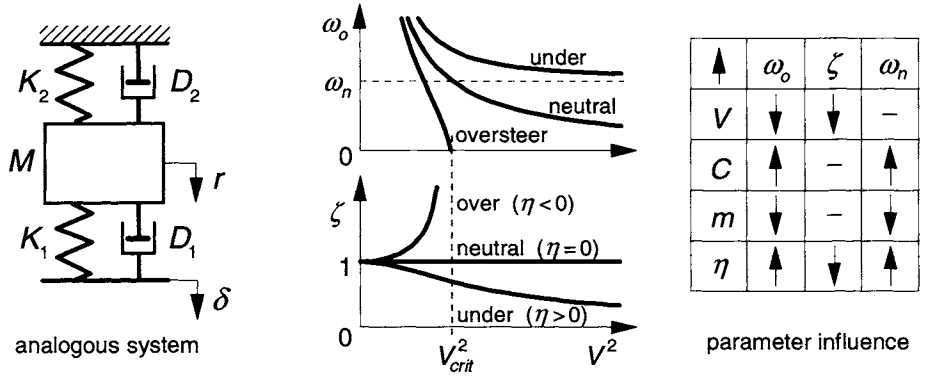

Fig. 1.13. The influence of parameters on natural frequency and damping.

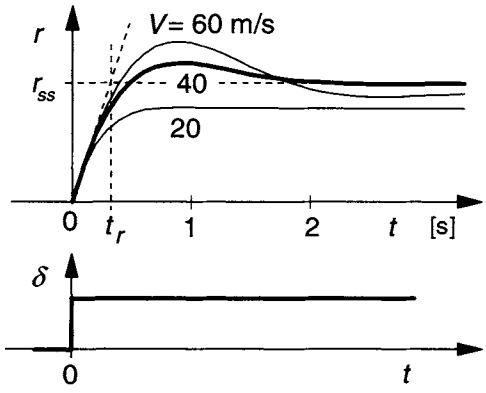

	t_r
$V<V_{char}$	↑
$V>V_{char}$	↓
η	↓
C_1	↓
m	↑
k	↑

Fig. 1.14. Step response of yaw rate to steer angle. Parameters according to Table 1.1. Parameter influence on the rise time t_r.

time t_r indicated in Fig.1.14 and expressed in terms of the parameters as follows:

$$t_r = \frac{r_{ss}}{\left(\frac{\partial r}{\partial t}\right)_{t=0}} = \frac{mk^2V}{aC_1l\left(1+\frac{\eta}{gl}V^2\right)} = \frac{mk^2V}{\frac{a}{l}\left\{C_1l^2+\left(b-a\frac{C_1}{C_2}\right)mV^2\right\}} \quad (1.73)$$

which expression may be readily obtained with the aid of Eqs.(1.46,1.47).

The parameter influence has been indicated in the figure. The results correspond qualitatively well with the 90% response times found in vehicle model simulation studies. A remarkable result is that for an understeered automobile the response time is smaller than for an oversteered car.

Forced Linear Vibrations

The conversion of the equations of motion (1.46) into the standard state space representation is useful when the linear system properties are the subject of investigation. The system at hand is of the second order and hence possesses two state variables for which we choose: v and r. The system is subjected to a single input signal: the steer angle δ. Various variables may be of interest to analyse the vehicle's response to steering input oscillations. The following quantities are selected to illustrate the method and to study the dynamic behaviour of the vehicle: the lateral acceleration a_y of the centre of gravity of the vehicle, the yaw rate r and the vehicle slip angle β defined at the centre of gravity. In matrix notation the equation becomes:

$$\dot{\boldsymbol{x}} = \boldsymbol{A}\boldsymbol{x} + \boldsymbol{B}\boldsymbol{u}$$
$$\boldsymbol{y} = \boldsymbol{C}\boldsymbol{x} + \boldsymbol{D}\boldsymbol{u} \tag{1.74}$$

with

$$\dot{\boldsymbol{x}} = \begin{pmatrix} \dot{v} \\ \dot{r} \end{pmatrix}, \quad \boldsymbol{u} = \delta, \quad \boldsymbol{y} = \begin{pmatrix} a_y \\ r \\ \beta \end{pmatrix} = \begin{pmatrix} \dot{v} + Vr \\ r \\ -v/V \end{pmatrix} \tag{1.75}$$

and

$$\boldsymbol{A} = -\begin{pmatrix} \dfrac{C}{mV} & V + \dfrac{Cs}{mV} \\ \dfrac{Cs}{mk^2V} & \dfrac{Cq^2}{mk^2V} \end{pmatrix}, \quad \boldsymbol{B} = \begin{pmatrix} \dfrac{C_1}{m} \\ \dfrac{C_1 a}{mk^2} \end{pmatrix}$$

$$\boldsymbol{C} = -\begin{pmatrix} \dfrac{C}{mV} & \dfrac{Cs}{mV} \\ 0 & -1 \\ 1/V & 0 \end{pmatrix}, \quad \boldsymbol{D} = \begin{pmatrix} \dfrac{C_1}{m} \\ 0 \\ 0 \end{pmatrix} \tag{1.76}$$

The frequency response functions have been computed using Matlab software. Figure 1.15 presents the amplitude and phase response functions for each of the three output quantities and at three different values of speed of travel. The values of the chosen model parameters and a number of characteristic quantities have been listed in Table 1.1.

Explicit expressions of the frequency response functions in terms of model parameters are helpful to understand and predict the characteristic aspects of these functions which may be established by means of computations or possibly through full scale experiments.

From the differential equation (1.50) the frequency response function is easily derived. Considering the quantities formulated by (1.70) and (1.71) and the steady-state response $(r/\delta)_{ss} = (V/R)/\delta$ obtained from (1.56) we find:

Table 1.1. Parameter values and typifying quantities

parameters		derived typifying quantities					
a	1.4 m	l	3 m	V [m/s]	20	40	60
b	1.6 m	F_{z1}	8371 N	ω_o [rad/s]	4.17	2.6	2.21
C_1	60000N/rad	F_{z2}	7325 N	ζ [-]	0.9	0.7	0.57
C_2	60000N/rad	q	1.503 m	ω_n [rad/s]	1.8	1.8	1.82
m	1600 kg	s	-0.1 m	t_r [s]	0.23	0.3	0.27
k	1.5 m	η	0.0174 rad (~1° extra steer / g lateral accel.)				

$$\frac{r}{\delta}(j\omega)=\left(\frac{r}{\delta}\right)_{ss}\cdot\frac{1+\dfrac{mVa}{C_2 l}j\omega}{1-\left(\dfrac{\omega}{\omega_o}\right)^2+2\zeta\left(\dfrac{j\omega}{\omega_o}\right)}\;;\quad\left(\frac{r}{\delta}\right)_{ss}=\frac{V/l}{1+\dfrac{\eta}{gl}V^2}\qquad(1.77)$$

Similarly, the formula for the response of lateral acceleration a_y can be derived:

$$\frac{a_y}{\delta}(j\omega)=\left(\frac{a_y}{\delta}\right)_{ss}\cdot\frac{1-\dfrac{mk^2}{C_2 l}\omega^2+\dfrac{b}{V}j\omega}{1-\left(\dfrac{\omega}{\omega_o}\right)^2+2\zeta\left(\dfrac{j\omega}{\omega_o}\right)}\;;\quad\left(\frac{a_y}{\delta}\right)_{ss}=\frac{V^2/l}{1+\dfrac{\eta}{gl}V^2}\qquad(1.78)$$

and for the slip angle β:

$$\frac{\beta}{\delta}(j\omega)=\left(\frac{\beta}{\delta}\right)_{ss}\cdot\frac{1-\dfrac{mk^2V}{amV^2-bC_2 l}j\omega}{1-\left(\dfrac{\omega}{\omega_o}\right)^2+2\zeta\left(\dfrac{j\omega}{\omega_o}\right)}\;;\quad\left(\frac{\beta}{\delta}\right)_{ss}=-\frac{b}{l}\frac{1-\dfrac{a}{b}\dfrac{m}{C_2 l}V^2}{1+\dfrac{\eta}{gl}V^2}\qquad(1.79)$$

By considering Eq.(1.77) it can now be explained that for instance at higher frequencies the system exhibits features of a first-order system: because of the $j\omega$ term in the numerator the yaw rate amplitude response tends to a decay at a 6dB per octave rate (when plotted in log-log scale) and the phase lag approaches

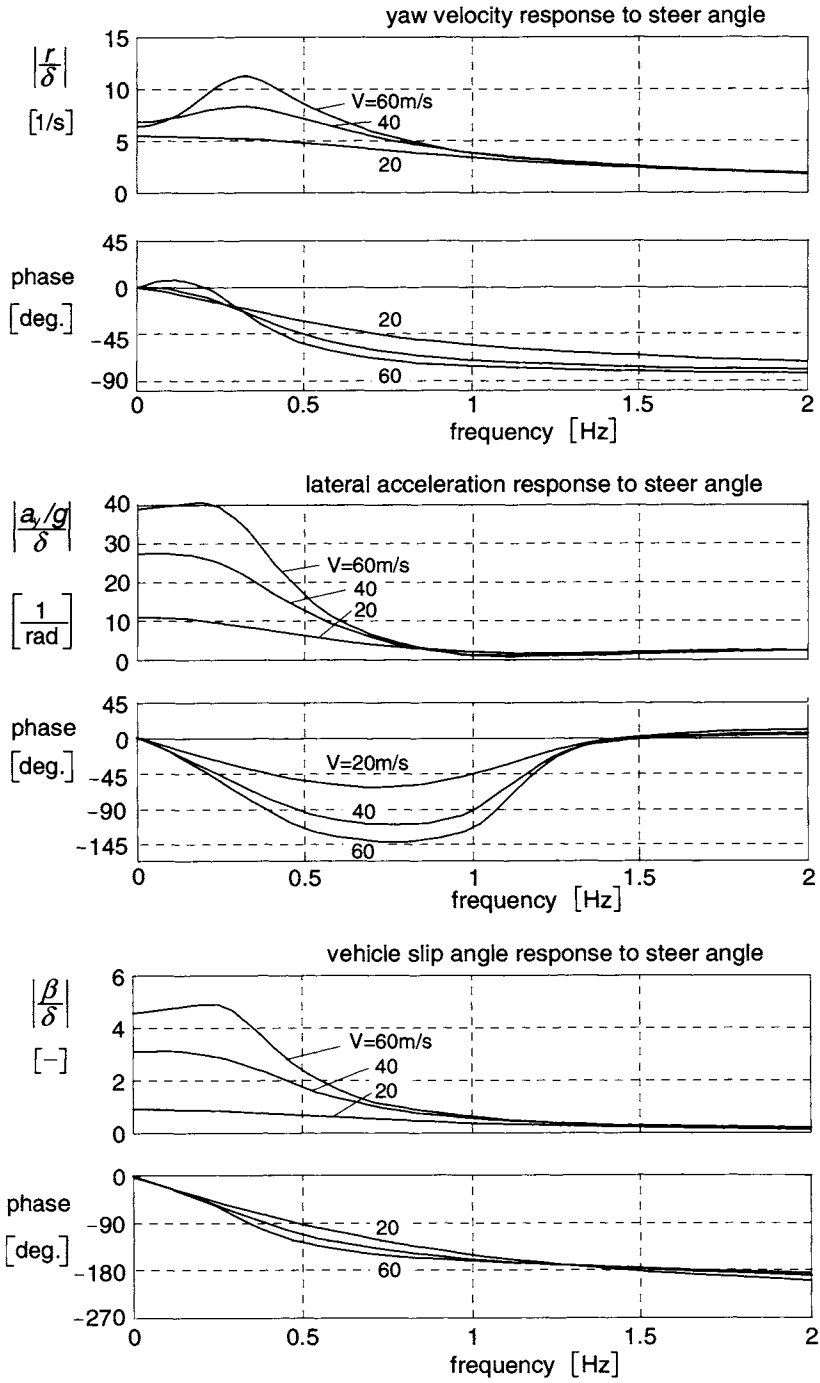

Fig. 1.15. Frequency response functions; vehicle parameters according to Table 1.1.

90 degrees. The phase increase at low frequencies and higher speeds is due to the presence of the speed V in that same term. At speeds beyond approximately the characteristic speed, the corresponding (last) term in the denominator has less influence on the initial slope of the phase characteristic. The lateral acceleration response (1.78) shown in the centre graph of Fig.1.15 gives a finite amplitude at frequencies tending to infinity because of the presence of ω^2 in the numerator. For the same reason, the phase lag goes back to zero at large frequencies. The side slip phase response tends to -270 degrees (at larger speeds) which is due to the negative coefficient of $j\omega$ in the numerator of (1.79). This in contrast to that coefficient of the yaw rate response (1.77).

It is of interest to see that the steady-state slip angle response, indicated in (1.79), changes sign at a certain speed V. At low speeds where the tyre slip angles are still very small, the vehicle slip angle obviously is negative for positive steer angle (considering positive directions as adopted in Fig.1.11). At larger velocities the tyre slip angles increase and as a result, β changes into the positive direction.

Exercise 1.2. Four-wheel steer, condition that the vehicle slip angle vanishes

Consider the vehicle model of Fig.1.16. Both the front and the rear wheels can be steered. The objective is to have a vehicle moving with a slip angle β remaining equal to zero. In practice, this may be done to improve handling qualities of the automobile (reduces to first-order system!) and to avoid excessive side slipping motions of the rear axle in lane change manoeuvres. Adapt the equations of motion (1.46) and assess the required relationship between the steer angles δ_1 and δ_2. Do this in terms of the transfer function between δ_2 and δ_1 and the associated differential equation. Find the steady-state ratio $(\delta_2/\delta_1)_{ss}$ and plot this as a function of the speed V. Show also the frequency response function $\delta_2/\delta_1(j\omega)$ for the amplitude and phase at a speed V=30 m/s. Use the vehicle parameters supplied in Table 1.1.

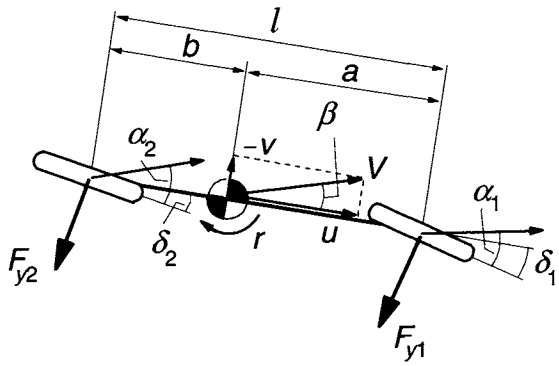

Fig. 1.16. 'Four-wheel' steering to make slip angle $\beta = 0$ (Exercise 1.2).

1.3.3. Non-Linear Steady-State Cornering Solutions

From Eqs.(1.42) and (1.59) with the same restrictions as stated below Eq.(1.60), the following force balance equations can be derived (follows also from Eqs.(1.61)). The effect of the pneumatic trails will be dealt with later on.

$$\frac{F_{y1}}{F_{z1}} = \frac{F_{y2}}{F_{z2}} = \frac{a_y}{g} \quad \left(= \frac{K}{mg} \right) \tag{1.80}$$

Where $K = ma_y$ represents the centrifugal force. The kinematic relationship

$$\delta - (\alpha_1 - \alpha_2) = \frac{l}{R} \tag{1.81}$$

follows from Eqs.(1.44) and (1.51). In Fig.1.11 the vehicle model has been depicted in a steady-state cornering manoeuvre. It can easily be observed from this diagram that relation (1.81) holds approximately when the angles are small.

The ratio of the side force and vertical load as shown in (1.80) plotted as a function of the slip angle may be termed as the normalised tyre or axle characteristic. These characteristics subtracted horizontally from each other produce the 'handling curve'. Considering the equalities (1.80) the ordinate may be replaced by a_y/g. The resulting diagram with abscissa $\alpha_1 - \alpha_2$ is the non-linear version of the right-hand diagram of Fig.1.10 (rotated 90° anti-clockwise). The diagram may be completed by attaching the graph that shows for a series of speeds V the relationship between lateral acceleration (in g units) a_y/g and the relative path curvature l/R according to Eq.(1.55).

Figure 1.17 shows the normalised axle characteristics and the completed handling diagram. The handling curve consists of a main branch and two side lobes. The different portions of the curves have been coded to indicate the corresponding parts of the original normalised axle characteristics they originate from. Near the origin the system may be approximated by a linear model. Consequently, the slope of the handling curve in the origin with respect to the vertical axis is equal to the understeer coefficient η. In contrast to the straight handling line of the linear system (Fig.1.10), the non-linear system shows a curved line. The slope changes along the curve which means that the degree of understeer changes with increasing lateral acceleration. The diagram of Fig.1.17 shows that the vehicle considered changes from understeer to oversteer. We define:

$$\begin{aligned} &\textit{understeer} \quad \text{if:} \quad \left(\frac{\partial \delta}{\partial V}\right)_R > 0 \\ &\textit{oversteer} \quad \text{if:} \quad \left(\frac{\partial \delta}{\partial V}\right)_R < 0 \end{aligned} \tag{1.82}$$

The family of straight lines represents the relationship between acceleration and curvature at different levels of speed. The speed line belonging to V= 50km/h has been indicated (wheel base l= 3m). This line is shifted to the left over a distance equal to the steer angle δ = 0.04rad and three points of intersection with the handling curve arise. These points I, II and III indicate the possible equilibrium conditions at the chosen speed and steer angle. The connected values of the relative path curvature l/R can be found by going back to the speed line. As will

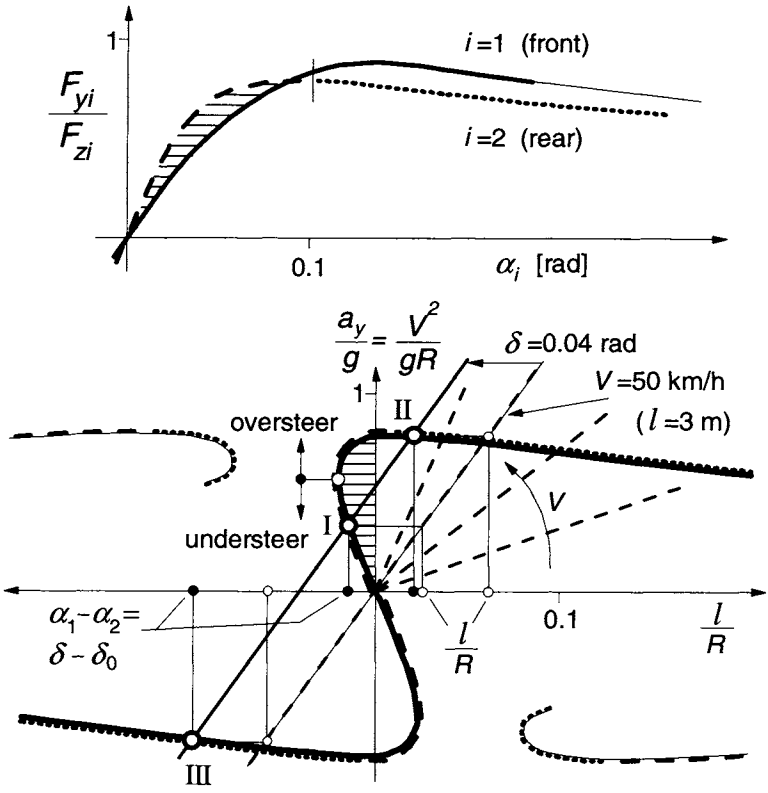

Fig. 1.17. Handling diagram resulting from normalised tyre characteristics. Equilibrium points I, II and III (steady turns) of which only I is stable, arise for speed V= 50 km/h and steer angle δ = 0.04 rad. From the different line types the manner in which the curves are obtained from the upper diagram may be retrieved.

be shown further on, only point I refers to a stable cornering motion. In points II and III ($R<0$!) the motion is unstable.

At a given speed V, a certain steer angle δ is needed to negotiate a circular path with given radius R. The steer angle required can be read directly from the handling diagram. The steer angle needed to negotiate the same curve at very low speed ($V \to 0$) tends to l/R. This steer angle is denoted with δ_0. Consequently, the abscissa of the handling curve $\alpha_1 - \alpha_2$ may as well be replaced by $\delta - \delta_0$. This opens the possibility to determine the handling curve with the aid of simple experimental means, i.e. measuring the steering wheel input (reduced to equivalent road wheel steer angle by means of the steering ratio, which method automatically includes steering compliance effects) at various speeds running over the same circular path.

Subtracting normalised characteristics may give rise to very differently

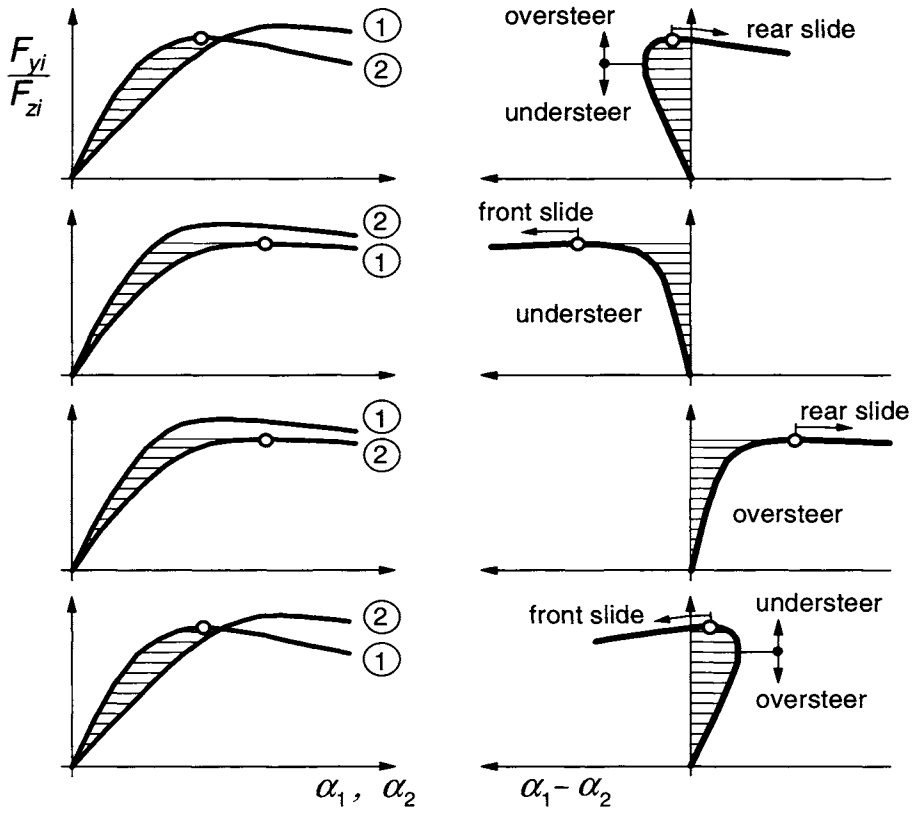

Fig. 1.18. A number of handling curves arising from the pairs of normalised tyre characteristics shown left. Only the main branch of the handling curve has been drawn (1: front, 2: rear).

shaped handling curves only by slightly modifying the original characteristics. As Fig.1.17 shows, apart from the main branch passing through the origin, isolated branches may occur. These are associated with at least one of the decaying ends of the pair of normalised tyre characteristics.

In Fig.1.18 a set of four possible combinations of axle characteristics have been depicted together with the resulting handling curves. This collection of characteristics shows that the nature of steering behaviour is entirely governed by the normalised axle characteristics and in particular their relative shape with respect to each other.

The way in which we can use the handling diagram is presented in Fig.1.19. The speed of travel may be kept constant and the lateral acceleration is increased by running over a spiral path with decreasing radius. The required variation of the steer angle follows from the distance between the handling curve and the speed line. Similarly we can observe what happens when the path curvature is kept constant and the speed is increased. Also, the resulting variation of the curvature at a constant steer angle and increasing speed can be found. More general cases of quasi steady-state motions may be studied as well.

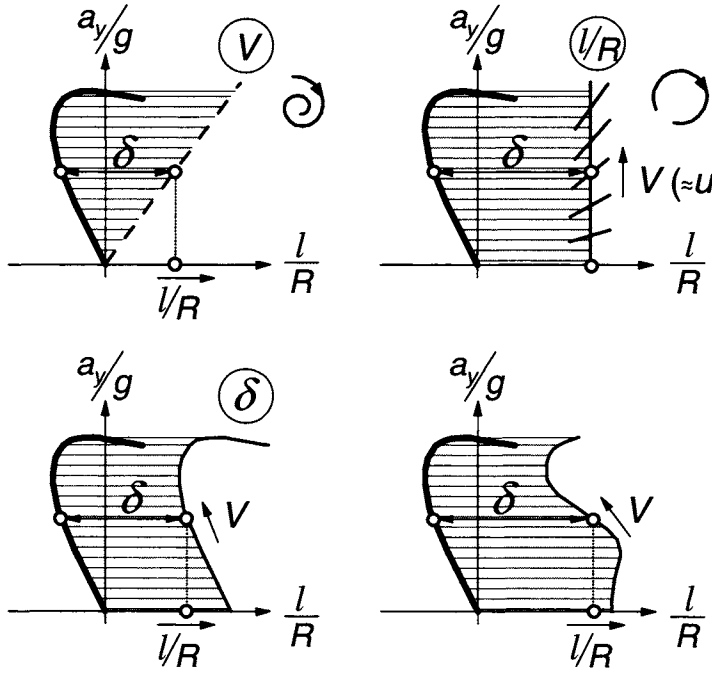

Fig. 1.19. Types of quasi steady-state manoeuvres.

Stability of the Motion at Large Lateral Accelerations

The non-linear set of equations (1.42-44) may be linearised around the point of operation, that is one of the equilibrium states indicated above. The resulting second-order differential equation has a structure similar to Eq.(1.64) or (1.47) but with the variables replaced by their small variations with respect to the steady-state condition considered. Analysis of the coefficients of the characteristic equation reveals if stability exists. Also the nature of stability (monotonous, oscillatory) follows from these coefficients. This is reflected by the type of singular points (node, spiral, saddle) representing the equilibrium solutions in the phase plane as treated in the next section.

It now turns out that not only the last coefficient can become negative but also the second coefficient a_1. Instead of the cornering stiffnesses C defined in the origin of the tyre cornering characteristics, the slope of the normalised characteristics at a given level of a_y/g becomes now of importance. We define

$$\Phi_i = \frac{1}{F_{zi}} \frac{\partial F_{yi}}{\partial \alpha_i} \qquad (i = 1, 2) \tag{1.83}$$

The conditions for stability, that is: second and last coefficient of equation comparable with Eq.(1.47) must be positive, read after having introduced the radius of gyration k ($k^2 = I/m$):

$$(k^2 + a^2)\Phi_1 + (k^2 + b^2)\Phi_2 > 0 \tag{1.84}$$

$$\Phi_1 \Phi_2 \left(\frac{\partial \delta}{\partial 1/R} \right)_V > 0 \tag{1.85}$$

The subscript V refers to the condition of differentiation with V kept constant, that is while staying on the speed line of Fig.1.17. The first condition (1.84) may be violated when we deal with tyre characteristics showing a peak in side force and a downwards sloping further part of the characteristic. The second condition corresponds to condition (1.65) for the linear model. Accordingly, instability is expected to occur beyond the point where the steer angle reaches a maximum while the speed is kept constant. This, obviously, can only occur in the oversteer range of operation. In the handling diagram the stability boundary can be assessed by finding the tangent to the handling curve that runs parallel to the speed line considered.

In the upper diagram of Fig.1.20 the stability boundary, that holds for the right part of the diagram (a_y vs l/R), has been drawn for the system of Fig.1.17 that changes from initial understeer to oversteer. In the middle diagram a number

of shifted V-lines, each for a different steer angle δ, has been indicated. In each case the points of intersection represent possible steady-state solutions. The highest point represents an unstable solution as the corresponding point on the speed line lies in the unstable area. When the steer angle is increased the two points of intersections move towards each other. It turns out that for this type of handling curve a range of δ values exists without intersections with the positive half of the curve. The fact that both right-hand turn solutions may vanish has serious implications which follows from the phase plot. At increased steer angle, however, new solutions may show up. At first, these solutions appear to be unstable, but at rather large steer angles of more than about 0.2rad we find again stable solutions. These occur on the isolated branch where α_2 is small and α_1 is large. Apparently, we find that the vehicle that increases its speed while running at a constant turning radius will first cross the stability boundary and may then

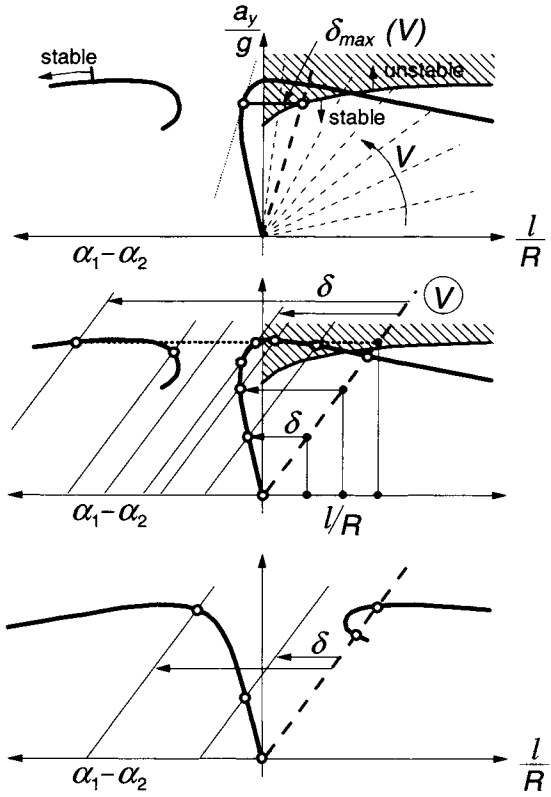

Fig. 1.20. Construction of stability boundary (upper diagram, from Fig.1.17). On the isolated branch a stable range may occur (large steer angle as indicated in middle diagram). The lower diagram shows the case with complete understeer featuring a stable main branch.

recover its stability by turning the steering wheel to a relatively large angle. In the diagram the left part of the isolated branch is reached where stable spirals appear to occur. This phenomenon may correspond to similar experiences in the racing practice, cf. Jenkinson (1958).

The lower diagram depicts the handling curve for a car that remains understeered throughout the lateral acceleration range. Everywhere the steady-state cornering motion remains stable. Up to the maximum of the curve the tangents slope to the left and cannot run parallel to a speed line. Beyond the peak, however, we can find a speed line parallel to the tangent, but at the same time one of the slopes (Φ_1) of the normalised axle characteristics starts to show a negative sign so that condition (1.85) is still satisfied. Similarly, the limit oversteer vehicle of the upper graph remains unstable beyond the peak. On the isolated part of the handling curve of the lower diagram the motion remains unstable. It will be clear that the isolated branches vanish when we deal with axle characteristics that do not show a peak and decaying part of the curve.

It may seem that the establishment of unstable solutions has no particular value. It will become clear, however, that the existence and the location of both stable and unstable singular points play an important role in shaping the trajectories in the phase-plane. Also, the nature of stability or instability in the singular points are of importance.

Exercise 1.3. Construction of the complete handling diagram from pairs of axle characteristics

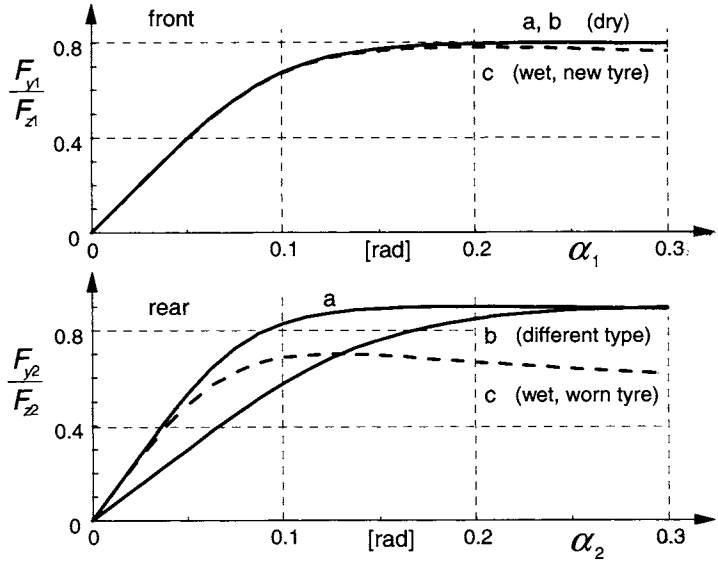

Fig. 1.21. Three sets of hypothetical axle cornering characteristics (Exercise 1.3).

We consider three sets of hypothetical axle characteristics (a, b and c) shown in the graph of Fig.1.21. The dimensions of the vehicle model are: $a = b = \frac{1}{2}l = 1.5$ m. For the tyres we may employ axle characteristics described by the *Magic Formula* (1.6):

$$F_y = D \sin[C \arctan\{B\alpha - E(B\alpha - \arctan(B\alpha))\}]$$

We define: the peak side force $D = \mu F_z$ and the cornering stiffness $C_{F\alpha} = BCD = c_{F\alpha} F_z$ so that $B = c_{F\alpha}/(C\mu)$. For the six tyre/axle configurations the parameter values have been given in the table below.

axle	case	μ	$c_{F\alpha}$	C	E
front	a, b	0.8	8	1.2	-2
	c	0.78	8	1.3	-2
rear	a	0.9	11	1.2	-2
	b	0.9	6	1.2	-2
	c	0.65	11	1.5	-1

Determine for each of the three combinations (two dry, one wet):

1. The handling curve (cf. Fig. 1.17).
2. The complete handling diagram (cf. Fig. 1.17).
3. The portion of the curves where the vehicle shows an oversteer nature.
4. The stability boundary (associated with these oversteer ranges) in the (a_y/g versus l/R) diagram (= right-hand side of the handling diagram) (cf. Fig.1.20).
5. Indicate in the diagram (or in a separate graph):
   a. the course of the steer angle δ required to negotiate a curve with radius $R = 60$m as a function of the speed V. If applicable, indicate the stability boundary, that is the critical speed V_{crit}, belonging to this radius.
   b. the course of steer angle δ as a function of relative path curvature l/R at a fixed speed $V = 72$ km/h and if applicable assess the critical radius R_{crit}.

For the vehicle systems considered so far a unique handling curve appears to suffice to describe the steady-state turning behaviour. Cases may occur, however, where more curves are needed, one for each velocity. A simple example is the situation when the car runs over a wet surface where the tyre characteristics change considerably with speed. Also, as a result of the down forces acting on e.g. the body of a racing car, the tyre loads increase with speed. Consequently, the tyre characteristics change accordingly which requires an adaptation of the handling curve.

A more difficult and fundamentally different situation occurs when the vehicle is equipped with a third axle. Also in this case multiple handling curves arise. A tandem rear axle configuration of a heavy truck for example, strongly opposes

movement along a curved track. The slip angles of the two rear axles are different so that a counteracting torque arises. This torque gets larger when the turning radius becomes smaller. This may for instance occur at a given level of lateral acceleration. When at this level the speed becomes lower, the curvature must become larger and the opposing torque will increase which entails an increased front steer angle to generate a larger side force needed to balance the vehicle. This increased steer angle goes on top of the steer angle which was already larger because of the increased *l/R*. Here, *l* is the average wheel base. Consequently, in the handling diagram, the points on the handling curve belonging to the lower speed lie more to the left. For a detailed study on this special subject we refer to Winkler (1998).

Assessment of the Influence of the Pneumatic Trail on the Handling Curve

So far the direct influence of the pneumatic trails have not been taken into account. As with the linear analysis we may do this by considering the effective axle positions

$$a'=a-t_1\,,\quad b'=b+t_2 \qquad \text{and} \qquad l'=a'+b' \tag{1.86}$$

The difficulty we have to face now is the fact that these pneumatic trails t_i will vary with the respective slip angles. We have if the residual torques are neglected:

$$t_i(\alpha_i) = -\frac{M_{zi}(\alpha_i)}{F_{yi}(\alpha_i)} \tag{1.87}$$

Introducing the effective axle loads

$$F'_{z1} = \frac{b'}{l'}mg\,,\quad F'_{z2} = \frac{a'}{l'}mg \tag{1.88}$$

yields for the lateral force balance instead of (1.80):

$$\frac{F_{y1}}{F'_{z1}} = \frac{F_{y2}}{F'_{z2}} = \frac{a_y}{g} \tag{1.89}$$

or after some rearrangements:

$$\frac{a'}{a}\frac{F_{y1}}{F_{z1}} = \frac{b'}{b}\frac{F_{y2}}{F_{z2}} = Q\frac{a_y}{g} \tag{1.90}$$

with

$$Q = \frac{l}{l'}\frac{a'b'}{a\,b} \approx 1 \tag{1.91}$$

The corrected normalised side force characteristics as indicated in (1.90) can be computed beforehand and drawn as functions of the slip angles and the normal procedure to assess the handling curve can be followed. This can be done by taking the very good approximation $Q=1$ or we might select a level of Qa_y/g then assess the values of the slip angles that belong to that level of the corrected normalised side forces and compute Q according to (1.91) and from that the correct value of a_y/g.

Large Deviations with Respect to the Steady-State Motion

The variables r and v may be considered as the two state variables of the second-order non-linear system represented by the equations (1.42). Through computer numerical integration the response to a given arbitrary variation of the steer angle can be easily obtained. For motions with constant steer angle δ (possibly after a step change), the system is autonomous and the phase-plane representation may be used to find the solution. For that, we proceed by eliminating the time from Eqs.(1.42). The result is a first-order non-linear equation (using $k^2 = I/m$):

$$\frac{dv}{dr} = k^2 \frac{F_{y1} + F_{y2} - mVr}{aF_{y1} - bF_{y2}} \tag{1.92}$$

Since F_{y1} and F_{y2} are functions of α_1 and α_2 it may be easier to take α_1 and α_2 as the state variables. With (1.44) we obtain:

$$\frac{d\alpha_2}{d\alpha_1} = \frac{dv/dr - b}{dv/dr + a} \tag{1.93}$$

which becomes with (1.92):

$$\frac{d\alpha_2}{d\alpha_1} = \frac{F_{y2}(\alpha_2)/F_{z2} - (\delta - \alpha_1 + \alpha_2)V^2/gl}{F_{y1}(\alpha_1)/F_{z1} - (\delta - \alpha_1 + \alpha_2)V^2/gl} \tag{1.94}$$

For the sake of simplicity we have assumed $I/m = k^2 = ab$.

By using Eq.(1.94) the trajectories (solution curves) can be constructed in the (α_1, α_2) plane. The isocline method turns out to be straightforward and simple to employ. The pattern of the trajectories is strongly influenced by the so-called singular points. In these points the motion finds an equilibrium. In the singular points the motion is stationary and consequently, the differentials of the state variables vanish.

From the handling diagram K/mg and l/R are readily obtained for given combinations of V and δ. Used in combination with the normalised tyre

characteristics F_{y1}/F_{z1} and F_{y2}/F_{z2} the values of α_1 and α_2 are found, which form the coordinates of the singular points. The manner in which a stable turn is approached and from what collection of initial conditions such a motion can or cannot be attained may be studied in the phase-plane. One of the more interesting results of such an investigation is the determination of the boundaries of the domain of attraction in case such a domain with finite dimensions exists. The size of the domain may give indications as to the so-called stability in the large. In other words the question may be answered: does the vehicle return to its original steady-state condition after a disturbance and to what degree does this depend on the magnitude and point of application of the disturbance impulse?

For the construction of the trajectories we draw isoclines in the (α_1, α_2) plane. These isoclines are governed by Eq.(1.94) with slope $d\alpha_2/d\alpha_1$ kept constant. The following three isoclines may already provide sufficient information to draw estimated courses of the trajectories. We have for $k^2 = ab$:

vertical intercepts $(d\alpha_2/d\alpha_1 \to \infty)$:

$$\alpha_2 = \frac{gl}{V^2}\frac{F_{y1}(\alpha_1)}{F_{z1}} + \alpha_1 - \delta \tag{1.95}$$

horizontal intercepts $(d\alpha_2/d\alpha_1 \to 0)$:

$$\alpha_1 = -\frac{gl}{V^2}\frac{F_{y2}(\alpha_2)}{F_{z2}} + \alpha_2 + \delta \tag{1.96}$$

intercepts under 45° $(d\alpha_2/d\alpha_1 = 1)$:

$$\frac{F_{y1}(\alpha_1)}{F_{z1}} = \frac{F_{y2}(\alpha_2)}{F_{z2}} \tag{1.97}$$

Figure 1.22 illustrates the way these isoclines are constructed. The system of Fig.1.17 with $k = a = b$, $\delta = 0.04$ rad and $V = 50$ km/h has been considered. Note, that the normalised tyre characteristics appear in the left-hand diagram for the construction of the isoclines. The three points of intersection of the isoclines are the singular points. They correspond to the points I, II and III of Fig.1.17. The stable point is a focus (spiral) point with a complex pair of solutions of the characteristic equation with a negative real part. The two unstable points are of the saddle type corresponding to a real pair of solutions, one of which is positive. The direction in which the motion follows the trajectories is still a question to be examined. Also for this purpose the alternative set of axes with r and v as coordinates (multiplied with a factor) has been introduced in the diagram after using the relations (1.44).

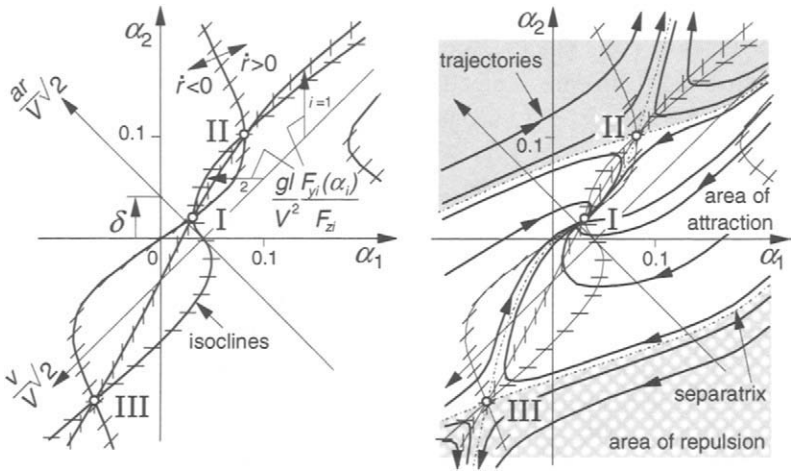

Fig. 1.22. Isoclines for the construction of trajectories in the phase-plane. Also shown: the three singular points I, II and III (cf. Fig.1.17) and the separatrices constituting the boundary of the domain of attraction. Point I represents the stable cornering motion at steer angle δ.

From the original equations (1.42) it can be found that the isocline (1.97) forms the boundary between areas with $\dot{r} > 0$ and $\dot{r} < 0$ (indicated in Fig.1.22). Now it is easy to ascertain the direction along the trajectories. We note that the system exhibits a bounded domain of attraction. The boundaries are called separatrices. Once outside the domain, the motion finds itself in an unstable situation. Remains the disturbance limited so that resulting initial conditions of the state variables stay within the boundaries, then ultimately the steady-state condition is reached again.

For systems with normalized characteristics showing everywhere a positive slope, a handling curve arises that consists of only the main branch through the origin. If the rear axle characteristic (at least in the end) is higher than the front axle characteristic, the vehicle will show (at least in the limit) an understeer nature and unstable singular points cannot occur. This at least if for the case of initial oversteer the speed remains under the critical speed. In such cases, the domain of attraction is theoretically unbounded so that for all initial conditions ultimately the stable equilibrium is attained. The domain of Fig.1.22 appears to be open on two sides which means that initial conditions, in a certain range of (r/v) values, do not require to be limited in order to reach the stable point. Obviously, disturbance impulses acting in front of the centre of gravity may give rise to such combinations of initial conditions.

In Figs.1.23 and 1.24 the influence of an increase in steer angle δ on the stability margin (distance between stable point and separatrix) has been shown

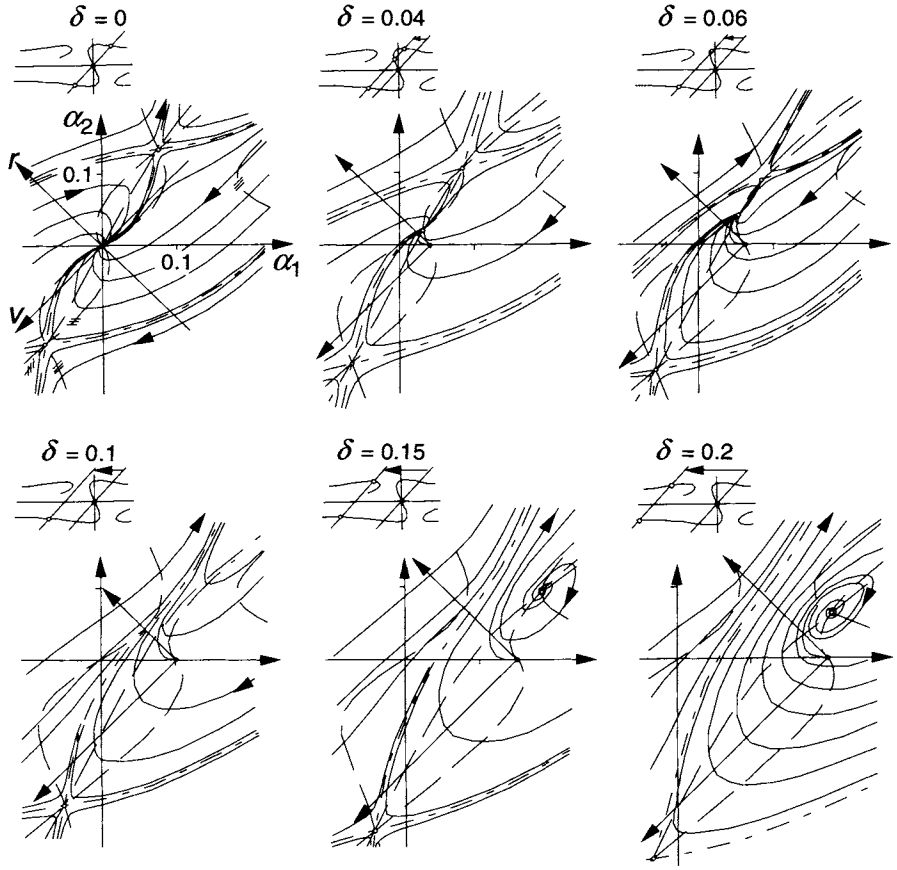

Fig. 1.23. Influence of steering on the stability margin (system of Fig.1.20 (top)).

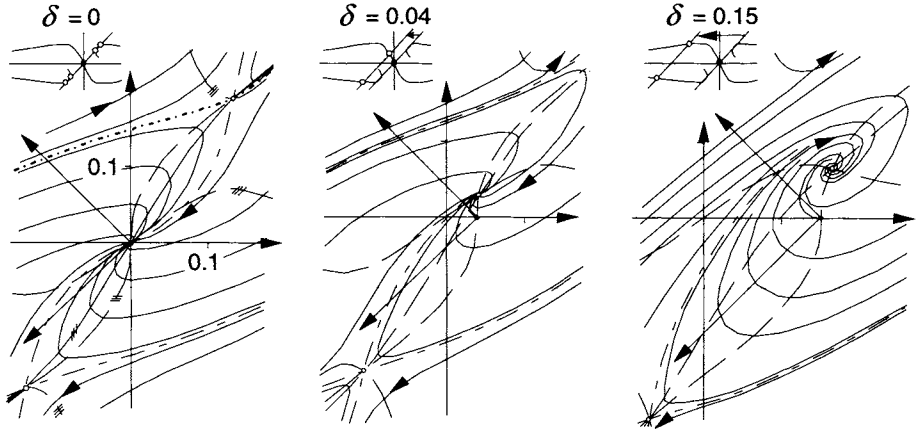

Fig. 1.24. Influence of steering on the stability margin (system of Fig.1.20 (bottom)).

for the two vehicles considered in Fig.1.20. The system of Fig.1.23 is clearly much more sensitive. An increase in δ (but also an increase in speed V) reduces the stability margin until it is totally vanished as soon as the two singular points merge (also the corresponding points I and II on the handling curve of Fig.1.17) and the domain breaks open. As a result, all trajectories starting above the lower separatrix tend to leave the area. This can only be stopped by either quickly reducing the steer angle or enlarging δ to around 0.2rad or more. The latter situation appears to be stable again (focus) as has been stated before. For the understeered vehicle of Fig.1.24 stability is practically always ensured.

For a further appreciation of the phase diagram it is of interest to determine the new initial state (r_o, v_o) after the action of a lateral impulse to the vehicle (cf. Fig.1.25). For an impulse S acting at a distance x in front of the centre of gravity the increase in r and v becomes:

$$\Delta r = \frac{Sx}{I} , \quad \Delta v = \frac{S}{m} \tag{1.98}$$

which results in the direction

$$\frac{a\Delta r}{\Delta v} = \frac{x}{b}\frac{ab}{k^2} \tag{1.99}$$

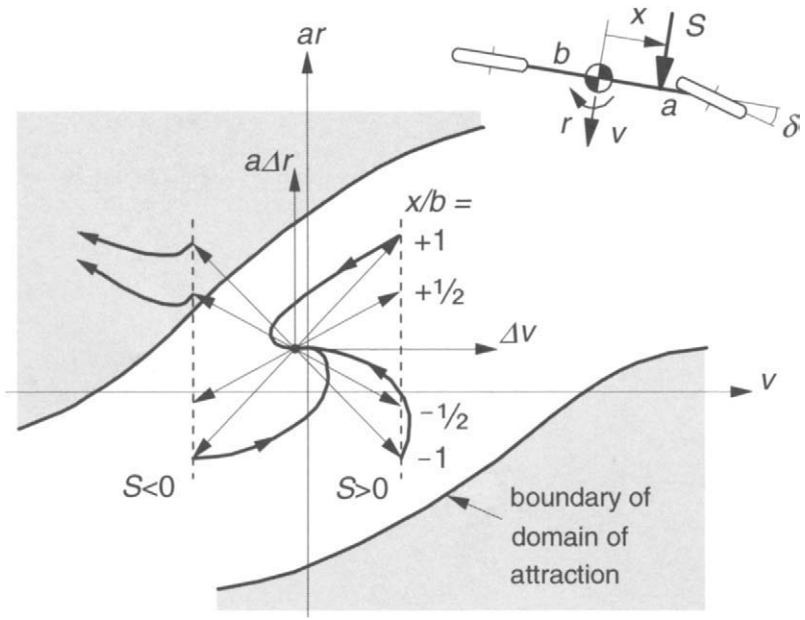

Fig. 1.25. Large disturbance in a curve. New initial state vector (Δv, Δr) after the action of a lateral impulse S. Once outside the domain of attraction the motion becomes unstable and may get out of control.

The figure shows the change in state vector for different points of application and direction of the impulse S ($k^2 = I/m = ab$). Evidently, an impulse acting at the rear (in outward direction) constitutes the most dangerous disturbance. On the other hand, an impulse acting in front of the centre of gravity about half way from the front axle does not appear to be able to get the new starting point outside of the domain of attraction no matter the intensity of the impulse.

When the slip angles become larger, the forward speed u may no longer be considered as a constant quantity. Then, the system is described by a third-order set of equations. In the paper (Pacejka 1986) the solutions for the simple automobile model have been presented also for yaw angles > 90°.

1.3.4. The Vehicle at Braking or Driving

When the vehicle is subjected to longitudinal forces that may result from braking or driving actions possibly to compensate for longitudinal wind drag forces or down or upward slopes, fore and aft load transfer will arise (Fig.1.26). The resulting change in tyre normal loads causes the cornering stiffnesses and the peak side forces of the front and rear axles to change. Since, as we assume here, the fore and aft position of the centre of gravity is not affected (no relative car body motion), we may expect a change in handling behaviour indicated by a rise or drop of the understeer gradient. In addition, the longitudinal driving or braking forces give rise to a state of combined slip, thereby affecting the side force in a way as shown in Fig.1.2.

For moderate driving or braking forces the influence of these forces on the side force F_y is relatively small and may be neglected for this occasion. This means that, for now, the cornering stiffness may be considered to be dependent on the normal load only. The upper left diagram of Fig.1.3 depicts typical

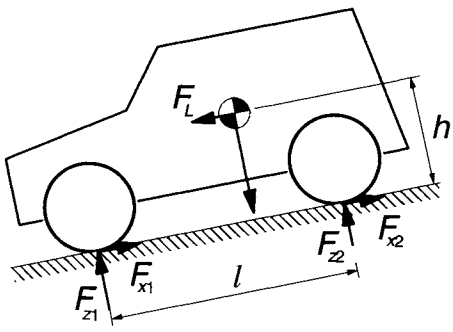

Fig. 1.26. The automobile subjected to longitudinal forces and the resulting load transfer.

variations of the cornering stiffness with vertical load.

The load transfer from the rear axle to the front axle that results from a forward longitudinal force F_L acting at the centre of gravity at a height h above the road surface (F_L possibly corresponding to the inertial force at braking) becomes:

$$\Delta F_z = \frac{h}{l} F_L \tag{1.100}$$

The understeer gradient reads according to Eq.(1.60):

$$\eta = \frac{F_{z1o}}{C_1(F_{z1})} - \frac{F_{z2o}}{C_2(F_{z2})} \tag{1.101}$$

The static axle loads F_{zio} (i=1 or 2) are calculated according to Eq.(1.59), while the actual loads F_{zi} front and rear become:

$$F_{z1} = F_{z1o} + \Delta F_z \ , \quad F_{z2} = F_{z2o} - \Delta F_z \tag{1.102}$$

At moderate braking with deceleration $-a_x = F_L/m$ the load transfer remains small and we may use the linearised approximation of the variation of cornering stiffness with vertical load:

$$C_i = C_{io} + \zeta_{\alpha i} \Delta F_{zi} \quad \text{with } \zeta_{\alpha i} = \left.\frac{\partial C_i}{\partial F_{zi}}\right)_{F_{zio}} \tag{1.103}$$

The understeer gradient (1.101) can now be expressed in terms of the longitudinal acceleration a_x (which might be: minus the forward component of the acceleration due to gravity parallel to the road). We obtain:

$$\eta = \eta_o + \lambda \frac{a_x}{g} \tag{1.104}$$

with the determining factor λ approximately expressed as:

$$\lambda = \zeta_{\alpha 1} \frac{h}{b} \left(\frac{F_{z1o}}{C_{1o}} \right)^2 + \zeta_{\alpha 2} \frac{h}{a} \left(\frac{F_{z2o}}{C_{2o}} \right)^2 \tag{1.105}$$

and η_o denoting the original value not including the effect of longitudinal forces. Obviously, since $\zeta_{\alpha 1,2}$ is usually positive, negative longitudinal accelerations a_x, corresponding to braking, will result in a decrease of the degree of understeer.

To illustrate the magnitude of the effect we use the parameter values given in Table 1.1 (above Eq.(1.77)) and add the c.g. height h=0.6m and the cornering stiffness versus load gradients $\zeta_{\alpha i} = 0.5 C_{io}/F_{zio}$. The resulting factor appears to take the value $\lambda = 0.052$. This constitutes an increase of η equal to $0.052 a_x/g$. Apparently, the effect of a_x on the understeer gradient is considerable when

regarding the original value $\eta_o = 0.0174$.

As illustrated by Fig.1.9 the peak side force will be diminished if a longitudinal driving or braking force is transmitted by the tyre. This will have an impact on the resulting handling diagram in the higher range of lateral acceleration. The resulting situation may be represented by the second and third diagrams of Fig.1.18 corresponding to braking (or driving) at the front or rear respectively. The problem becomes considerably more complex when we realise that at the front wheels the components of the longitudinal forces perpendicular to the x axis of the vehicle are to be taken into account. Obviously, we find that at braking of the front wheels these components will counteract the cornering effect of the side forces and thus will make the car more understeer. The opposite occurs when these wheels are driven (more oversteer). For a more elaborate discussion on this item we may refer to Pacejka (1973b).

At hard braking, possibly up to wheel lock, stability and steerability may deteriorate severely. This more complex situation will be discussed in Chapter 3 where more information on the behaviour of tyres at combined slip is given.

1.3.5. The Moment Method

Possible steady-state cornering conditions, stable or unstable, have been portrayed in the handling diagram of Fig.1.17. In Fig.1.22 motions tending to or departing from these steady-state conditions have been depicted. These motions are considered to occur after a sudden change in steer angle. The potential available to deviate from the steady turn depends on the margin of the front and rear side forces to increase in magnitude. For each point on the handling curve it is possible to assess the degree of manoeuvrability in terms of the moment that can be generated by the tyre side forces about the vehicle centre of gravity. Note that at the steady-state equilibrium condition the tyre side forces are balanced with the centrifugal force and the moment equals zero.

In general, the handling curve holds for a given speed of travel. That is so, when e.g. the aerodynamic down forces are essential in the analysis. In Fig.1.27 a diagram has been presented that is designated as the *MMM* diagram (the Milliken Moment Method diagram) and is computed for a speed of 60 mph. The force-moment concept was originally proposed by W.F.Milliken in 1952 and thereafter continuously further developed by the Cornell Aeronautical Laboratory staff and by Milliken Research Associates. A detailed description is given in Milliken's book (1995).

The graph shows curves of the resulting tyre moment N vs the resulting tyre side force Y in non-dimensional form. The resulting force and moment result

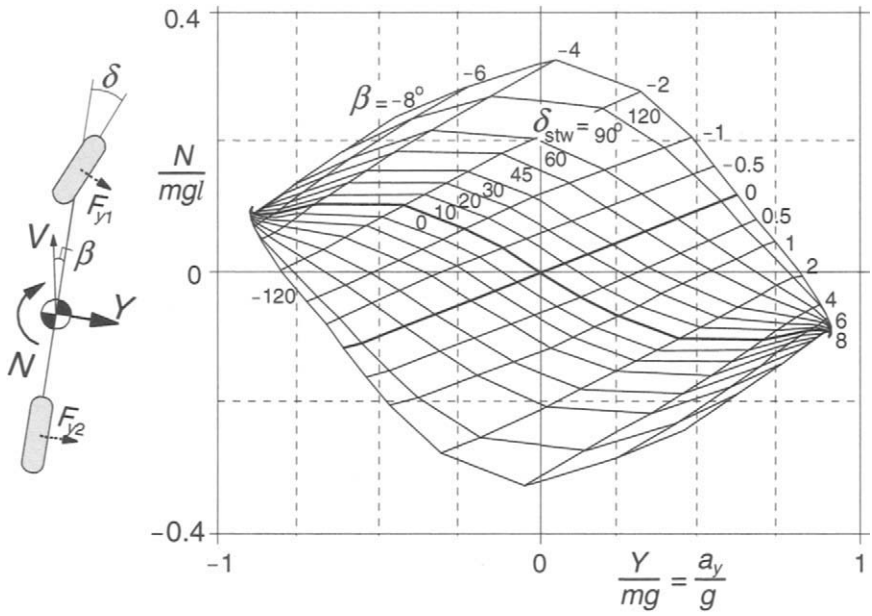

Fig. 1.27. The *MMM* diagram portraying the car's potential manoeuvring capacity.

from the individual side forces and act from ground to vehicle. For greater accuracy, one may take the effect of the pneumatic trails into consideration. Two sets of curves have been plotted: one set for constant values of the vehicle side slip angle β with the steering wheel angle δ_{stw} as parameter and the other set for contant steer angle and varying slip angle. Along the horizontal axis the moment is zero and we have the steady-state equilibrium cornering situation that corresponds with the handling curve. It is observed that for the constant speed considered in the diagram, the steer angle increases when the total side force Y or lateral acceleration a_y is chosen larger which indicates that the motion remains stable. At the limit (near number 2) the maximum steady-state lateral acceleration is attained. At that point the ability to generate a positive moment is exhausted. Only a negative moment may still be developed by the car that tends to straighten the curve that is being negotiated. As we have seen in Fig.1.18, second diagram, there is still some side force margin at the rear tyre which can be used to increase the lateral acceleration in a transient fashion. At the same time, however, the car yaws outwards because the associated moment is negative (cf. diagram near number 8). How to get at points below the equilibrium point near the number 2 is a problem. Rear wheel steering is an obvious theoretical option. In that way, the vehicle slip angle β and front steer angle δ can remain unchanged while the rear steer angle produce the desired rear tyre slip angle. Of course, the diagram needs to be adapted in case of rear wheel

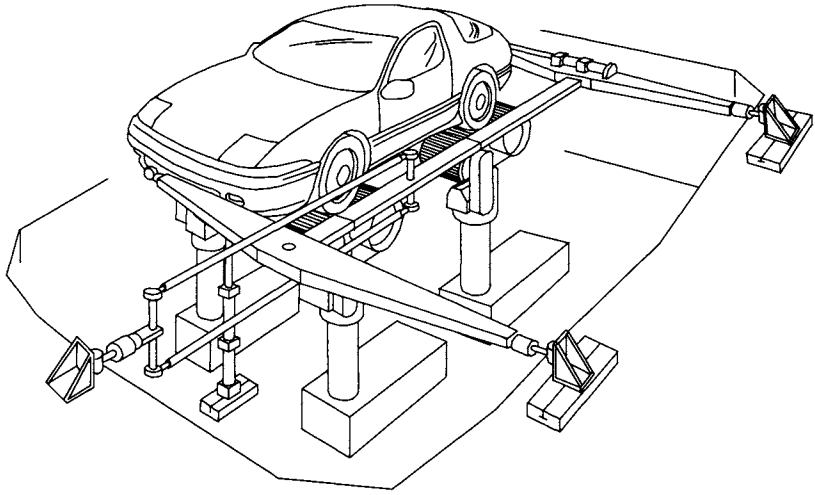

Fig. 1.28. The MTS Flat-Trac Roadway Simulator™, Milliken (1995).

steering. Another more practical solution would be to bring the vehicle in the desired attitude ($\beta \rightarrow 8°$) by briefly inducing large brake or drive slip at the rear that lowers the cornering force and lets the car swing to the desired slip angle while at the same time the steering wheel is turned backwards to even negative values.

The *MMM* diagram, which is actually a Gough plot (for a single tyre, cf. Figs.3.5 and 3.29) established for the whole car at different steer angles, may be assessed experimentally either through outdoor or indoor experiments. On the proving ground a vehicle may be attached at the side of a heavy truck or railway vehicle and set at different slip angles while the force and moment are being measured (tethered testing), cf. Milliken (1995). Figure 1.28 depicts the remarkable laboratory MMM test machine. This MTS Flat-Trac Roadway Simulator™ uses four flat belts which can be steered and driven independently. The car is constrained in its centre of gravity but is free to roll and pitch.

1.3.6. The Car-Trailer Combination

In this section we will discuss the role of the tyre in connection with the dynamic behaviour of a car that tows a trailer. More specifically, we will study the possible unstable motions that may show up with such a combination. Linear differential equations are sufficient to analyse the stability of the straight ahead motion. We will again employ Lagrange's equations to set up the equations of motion. The original equations (1.25) may be employed because the yaw angle

is assumed to remain small. The generalised coordinates Y, ψ and θ are used to describe the car's lateral position and the yaw angles of car and trailer respectively. The forward speed dX/dt ($\approx V \approx u$) is considered to be constant. Figure 1.29 gives a top view of the system with three degrees of freedom. The alternative set of three variables v, r and the articulation angle φ and the vehicle velocity V (a parameter) which are not connected to the inertial axes system (0, X, Y) has been indicated as well and will be employed later on. The kinetic energy for this system becomes, if we neglect all the terms of the second order of magnitude (products of variables):

$$T = \tfrac{1}{2}m(\dot{X}^2 + \dot{Y}^2) + \tfrac{1}{2}I\dot{\psi}^2 + \tfrac{1}{2}m_c\{\dot{X}^2 + (\dot{Y} - h\dot{\psi} - f\dot{\theta})^2\} + \tfrac{1}{2}I_c\dot{\theta}^2 \qquad (1.106)$$

The potential energy remains zero:

$$U = 0 \qquad (1.107)$$

and the virtual work done by the external road contact forces acting on the three axles reads:

$$\delta W = F_{y1}\delta(Y + a\psi) + F_{y2}\delta(Y - b\psi) + F_{y3}\delta(Y - h\psi - g\theta) \qquad (1.108)$$

With the use of the equations (1.25) and (1.29) the following equations of motion are established for the generalised coordinates Y, ψ and θ:

$$(m + m_c)\ddot{Y} - m_c(h\ddot{\psi} + f\ddot{\theta}) = F_{y1} + F_{y2} + F_{y3} \qquad (1.109)$$

$$(I_c + m_c f^2)\ddot{\theta} - m_c f(\ddot{Y} - h\ddot{\psi}) = -gF_{y3} \qquad (1.110)$$

$$(I + m_c h^2)\ddot{\psi} - m_c h(\ddot{Y} - f\ddot{\theta}) = aF_{y1} - bF_{y2} - hF_{y3} \qquad (1.111)$$

This constitutes a system of the sixth order. By introducing the velocities v and

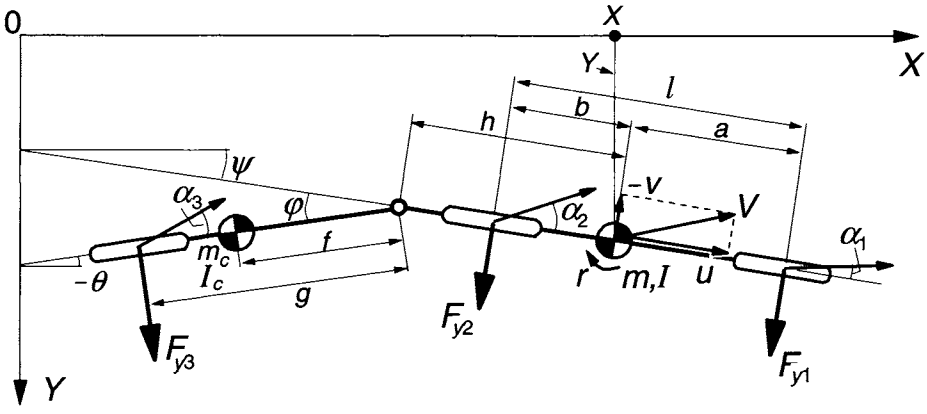

Fig. 1.29. Single track model of car trailer combination.

r the order can be reduced to four. In addition, the angle of articulation φ will be used. We have the relations:

$$\dot{Y} = V\psi + v \quad , \quad \dot{\psi} = r \quad , \quad \theta = \psi - \varphi \tag{1.112}$$

and with these the equations for v, r and φ:

$$(m + m_c)(\dot{v} + Vr) - m_c\{(h+f)\dot{r} - f\ddot{\varphi}\} = F_{y1} + F_{y2} + F_{y3} \tag{1.113}$$

$$\{I + m_c h(h+f)\}\dot{r} - m_c h(\dot{v} + Vr + f\ddot{\varphi}) = aF_{y1} - bF_{y2} - hF_{y3} \tag{1.114}$$

$$(I_c + m_c f^2)(\ddot{\varphi} - \dot{r}) + m_c f(\dot{v} + Vr - h\dot{r}) = gF_{y3} \tag{1.115}$$

The right-hand members are still to be expressed in terms of the motion variables. With the axle cornering stiffnesses C_1, C_2 and C_3 we have:

$$\begin{aligned} F_{y1} &= C_1\alpha_1 = -C_1\frac{v + ar}{V} \\ F_{y2} &= C_2\alpha_2 = -C_2\frac{v - br}{V} \\ F_{y3} &= C_3\alpha_3 = -C_3\left(\frac{v - hr - g(r - \dot{\varphi})}{V} + \varphi\right) \end{aligned} \tag{1.116}$$

From the resulting set of linear differential equations the characteristic equation may be derived which is of the fourth degree. Its general structure is:

$$a_0 s^4 + a_1 s^3 + a_2 s^2 + a_3 s + a_4 = 0 \tag{1.117}$$

The stability of the system can be investigated by considering the real parts of the roots of this equation or we might employ the criterium for stability according to Routh-Hurwitz. According to this criterium, the system of order n is stable when all the coefficients a_i are positive and the Hurwitz determinants H_{n-1}, H_{n-3} etc. are positive. For our fourth-order system the complete criterium for stability reads:

$$H_3 = \begin{vmatrix} a_1 & a_0 & 0 \\ a_3 & a_2 & a_1 \\ 0 & a_4 & a_3 \end{vmatrix} = a_1 a_2 a_3 - a_1^2 a_4 - a_0 a_3^2 > 0 \tag{1.118}$$

$$a_i > 0 \qquad \text{for } i = 0, 1, \ldots..4$$

In Fig.1.30, the boundaries of stability have been presented in the caravan axle cornering stiffness vs speed parameter plane. The three curves belong to the

three different sets of parameters for the position f of the caravan's centre of gravity and the caravan's mass m_c as indicated in the figure. An important result is that a lower cornering stiffness promotes oscillatory instability: the critical speed beyond which instability occurs decreases. Furthermore, it appears from the diagram that moving the caravan's centre of gravity forward (f smaller) stabilises the system which is reflected by the larger critical speed. A heavier caravan (m_c larger) appears to be bad for stability. Furthermore, it has been found that a larger draw bar length g is favourable for stability.

It turns out that a second type of instability may show up. This occurs when the portion of the weight of the caravan supported by the coupling point becomes too large. This extra weight is felt by the towing vehicle and makes it more oversteer. The critical speed associated with this phenomenon is indicated in the diagram by the vertical lines. This divergent instability occurs when (starting out from a stable condition) the last coefficient becomes negative, that is $a_n = a_4 < 0$.

The oscillatory instability connected with the 'snaking' phenomenon arises as soon as (from a stable condition) the second highest Hurwitz determinant becomes negative, $H_{n-1} = H_3 < 0$ (then also $H_n < 0$), cf. Klotter (1960) or Leipholz (1987). When the critical speed is surpassed self-excited oscillations are created which shows an amplitude that in the actual non-linear case does not appear to limit itself. This is in contrast to the case of the wheel shimmy phenomenon to

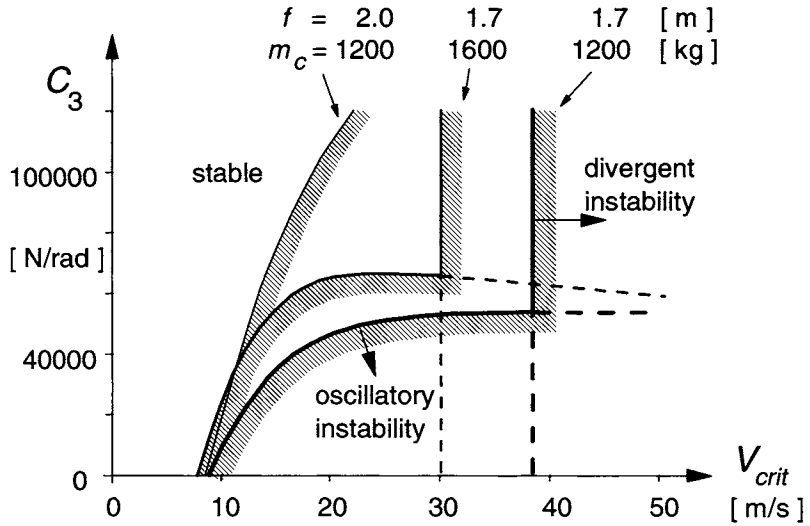

Fig. 1.30. Stability boundaries for the car caravan combination in the caravan cornering stiffness vs critical speed diagram. Vehicle parameters according to Table 1.1, in addition: $h = 2\text{m}$, $g = 2\text{m}$, $k_c = 1.5\text{m}$ ($I_c = m_c k_c^2$), cf. Fig.1.29.

be treated in Chapter 5 where a stable limited oscillation appears to arise. The cause of the unlimited snaking oscillation is that with increasing amplitudes also the slip angle increases which lowers the average cornering stiffness as a consequence of the degressively non-linear cornering force characteristic. From the diagram we found that this will make the situation increasingly worse. As has been seen from full vehicle/caravan model simulations, the whole combination will finally overturn. Another effect of this reduction of the average cornering stiffness is that when the vehicle moves at a speed lower than the critical speed, the originally stable straight ahead motion may become unstable if through the action of an external disturbance (side wind gust) the slip angle of the caravan axle becomes too large (surpassing of the associated unstable limit-cycle). This is an unfortunate, possibly dangerous situation! We refer to Troger and Zeman (1984) for further details.

Exercise 1.4. Stability of a trailer

Consider the trailer of Fig.1.31 that is towed by a heavy steadily moving vehicle at a forward speed V along a straight line. The trailer is connected to the vehicle by means of a hinge. The attachment point shows a lateral flexibility that is represented by the lateral spring with stiffness c_y. Furthermore, a yaw torsional spring and damper are provided with coefficients c_φ and k_φ.

Derive the equations of motion of this system with generalised coordinates y and φ. Assume small displacements so that the equations can be kept linear. The damping couple $k_\varphi\dot{\varphi}$ may be considered as an external moment acting on the trailer or we may use the dissipation function $D = \frac{1}{2} k_\varphi \dot{\varphi}^2$ and add $+\partial D/\partial \dot{q}_i$ to the left-hand side of Lagrange's equation (1.25). Obviously, the introduction of this extra term will be beneficial particularly when the system to be modelled is more complex.

Assess the condition for stability for this fourth-order system. Simplify the system by putting $g = f$ and $c_\varphi = k_\varphi = 0$. Now find the explicit conditional statement for the cornering stiffness C.

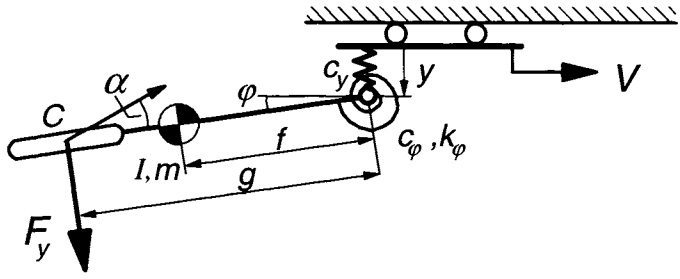

Fig. 1.31. On the stability of a trailer (Exercise 1.4).

1.3.7. Vehicle Dynamics at More Complex Tyre Slip Conditions

So far, relatively simple vehicle dynamics problems have been studied in which the basic steady-state cornering force versus slip angle characteristic plays the dominant role. The situation becomes more complex when matters like combined slip at hard braking, wheel camber, tyre transient and vibrational properties and e.g. obstacle crossings are to be considered.

In the subsequent chapters tyre performance and modelling will be treated in greater detail which enables us to introduce relevant tyre properties in the analysis. The following specific subjects will be studied as applications of the tyre modelling theory:

- Vehicle stability at excessive braking and wheel lock (Chapter 3)
- Motorcycle steady-state cornering (Chapter 11)
- Wheel shimmy (Chapter 6)
- Steering vibrations (Chapter 8)
- Motorcycle weave and wobble (Chapter 11)
- Tyre out-of-roundness (Chapter 8)
- Cornering on uneven roads (Chapters 5,8)
- ABS on uneven roads (Chapter 8)
- Traversing short obstacles (Chapter 10)
- Parking (Chapter 9)